Global regulation via modulation of ribosome pausing by EttA

Farès Ousalem[1§], Saravuth Ngo[1], Thomas Oïffer[1], Amin Omairi-Nasser[1],

Marion Hamon[2], Laura Monlezun[1], Grégory Boël[1,*]

[1]Expression Génétique Microbienne, CNRS, Université Paris Cité, Institut de Biologie Physico-Chimique, Paris, France. [2]Centre National de la Recherche Scientifique (CNRS), Institut de Biologie Physico-Chimique, Plateforme de Protéomique, FR550, F-75005 Paris, France.

[*] To whom correspondence may be addressed:
Grégory Boël, Institut de Biologie Physico-Chimique, 13 rue Pierre et Marie Curie, 75005 Paris, France, Tel: +33-1-58415121; e-mail: boel@ibpc.fr

Keywords: Protein synthesis, Acidic residues translation stalling, ABC-F protein family, TCA cycle, glyoxylate shunt.

[§] Current address: Biomarqueurs et nouvelles cibles thérapeutiques en oncologie, INSERM U981, Université Paris Saclay, Institut de Cancérologie Gustave Roussy, 11 rue Edouard Vaillant, 94805 Villejuif Cedex, France

Abstract

Having multiple rounds of translation of the same mRNA is a key feature of the Central Dogma that creates substantial dynamic complexities along with opportunities for regulation related to ribosome pausing and stalling at specific sequences[1-5]. The molecular mechanisms controlling these critical processes and the principles guiding their evolution remain among the least understood facets of cellular physiology. We herein use a combination of genetic, genomic, physiological, and biochemical methods to show that regulation of ribosome pausing at specific amino acid sequences can produce ~2-fold changes in protein expression levels that have a strong influence on cell growth and therefore evolutionary fitness. We demonstrate, both *in vivo* and *in vitro,* that the ABC-F protein EttA[6,7] directly controls the translation of mRNAs coding for a subset of enzymes in the tricarboxylic acid (TCA) cycle and its glyoxylate shunt, which dramatically modulates growth in some chemical environments. It also modulates expression of specific proteins involved in metabolically related physiological and stress-response pathways. These regulatory activities are mediated by EttA rescuing ribosomes paused at specific patterns of negatively charged residues within the first 30 amino acids of nascent proteins. The previously established dependency of EttA's activity on ADP:ATP ratio[6,7] can modulate these effects based on cellular energy status. We thus establish a new global regulatory paradigm based on sequence-specific modulation of translational pausing.

Main

The ATP binding protein F (ABC-F) family, belonging to the ABC superfamily[8], constitutes a group of proteins where all the members studied to date are involved in ribosome-related functions[6,7,9-12,9-21]. They are widespread in bacteria and eukaryotes and in general, paralogues are present in the same organism, such as *E. coli* which has four ABC-F proteins: EttA, Uup, YheS and YbiT[6,13,21-23].

ABC-F proteins are composed of two ABC domains in tandem connected together by a linker region that contains the P-site tRNA Interaction Motif (PtIM)[6,14,21,23,24], a signature motif of the family defined by the Pfam database[25] as ABC_tran_Xtn (PF12848). Each ABC-domain carries consensus Walker A and B motifs and in the presence of ATP the two domains come together, binding two ATP molecules to shape an ATP-bound closed conformation[21,23,26]. In this conformation, ABC-F proteins bind to the E site of the 70S ribosome[6,7,10,16,17,19,20] and require the hydrolysis of the ATP molecules to dissociate from the ribosome[6]. Consequently, an ATPase-deficient mutant, in which the two catalytic glutamates of each Walker B motif of the ABC domain are replaced by glutamines (EQ_2 mutant)[26], forms a stable complex with the ribosome[6,7,10,13,19,20]. This stabilization leads to an inhibition of protein synthesis and an arrest of bacterial growth[6,13,22]. To date, twelve cryo electron microscopy structures of ABC-F proteins in complex with the 70S ribosome are known. These structures reveal an overall geometry with similar contacts between the protein and the ribosome, but the corresponding regions of each ABC-F that contact the ribosome differ in sequences[7,10,12,16,19,20,23,27]. The PtIM extension points towards the peptidyl transfer center (PTC) of the ribosome, but shows considerable variation in length[10,16,17,19-21,28]. With the EF-P/eIF-5A protein that has been identified to rescue ribosomes stalled during the synthesis of polyproline-containing proteins[29-31], ABC-F are the only factors known to bind to the ribosomal E site.

Some ABC-F have a clear physiological function such as the antibiotic resistance ABC-F (ARE ABC-F) factors[9,10,12,14-20,32,33] which provide resistance toward antibiotics that target the PTC

and the nascent peptide exit tunnel (NPET) of the ribosome[9,10,12,16,17,19,20]. However, for most of the family, their physiological function remains unclear. In eukaryotes, ABC-F proteins are associated with pleiotropic effects. In yeast the N-terminal domain of GCN20 is involved in the regulation of translation upon amino-acid starvation[34,35]. The second yeast ABC-F, ARB1, is an essential gene important for ribosome biogenesis[36] and the corresponding protein has been identified in the cryo-EM structure of the 60S ribosomal quality control complex in a pre-peptidyl-tRNA cleavage state[28]. The human ABC50 (ABC-F1) protein influences translation initiation *in vitro* at an internal ribosome entry site of mRNA[37] and also functions as an E2 Ubiquitin-conjugating enzyme in the regulation of the inflammatory response in macrophages[38]. The three human ABC-F paralogues have been detected in processes involved in immune responses[39-44] and cancer developments and treatments[42,45-52], but their mechanism of action is unknown. In prokaryotes, all the structurally studied ABC-F can adjust the conformation of the PTC and/or the positioning of the P-site tRNA[13,23] (and some affect bacterial fitness[22]). Based on biochemical and structural studies of the EttA protein, we previously proposed a model in which EttA regulates the first step of translation depending on the ADP:ATP ratio in the reaction[6,7] and showed that loss of EttA resulted in reduced competitive fitness in stationary phase[6]. However, important questions remained: what is the physiological role of EttA in *E. coli* and does its action impact translation of all mRNA?

In this study we have used an unbiased approach to determine the impact of the *ettA* deletion (Δ*ettA*) on the physiology of *E. coli*. The gene deletion creates a hypersensitivity to salt when the bacteria are grown on carbon sources metabolized by the TCA cycle. This phenotype is due to the reduced translation of several genes of the TCA cycle and of genes involved in stress responses. For eight of them, we show that the reduced synthesis occurs during translation of their mRNAs when the newly polymerized protein contains acidic-amino acids within the first 30 amino acids *i.e.* before the elongating peptide reaches the end of the ribosomal NPET. We demonstrate that changes in the expression of *aceB* and *aceA* can explain most of the phenotypes we observed.

In addition, we show that over-expression of *mgtA* gene (encoding a Mg^{2+} transporter) in the Δ*ettA* strain is due to the action of EttA on the Intrinsic Ribosome Destabilization (IRD) effect of the leader peptide MgtL which regulates *mgtA* expression[3].

Loss of ettA impairs bacterial metabolic adaptation and alters protein expression patterns. Our investigation of the physiological function of EttA started with the previously reported phenotype of competitive fitness defect of the *ettA* deleted strain (Δ*ettA*) during extended stationary phase in LB[6]. In our replication of the experiment we discerned the phenotype's dependency on the source of the LB medium used (**Extended Data Fig. 1a**). Subsequently, we have now developed a MOPS-Tricine buffered minimal medium where the phenotype is enhanced, first by reducing the amount of inorganic phosphate, then by using amino acids (aa) as carbon source (MMAA medium) and finally by adding NaCl (0.4 M) to the medium (MMAA-NaCl). In this last condition, there was a rapid loss in competitive fitness of the Δ*ettA* strain compared to the previous condition (1 day vs 3 days) (**Extended Data Fig. 1a**). In this work we have systematically compared three strains MG1655 WT, Δ*ettA* and the Δ*ettA* complemented with an exogenous chromosomal copy of *ettA* (C_{ettA}). In the MMAA medium, all 3 strains doubled every 3 h, whereas in the MMAA-NaCl medium the doubling time of the WT and the complemented strains increased to 8 h (**Fig. 1a**) while that of the Δ*ettA* strain was more than 9 h and exhibited a much longer lag time (5 h) compared to the two other strains (**Fig. 1a**). Strains deleted for the other *E. coli* ABC-F genes, grew like the WT, showing that this phenotype is specific to *ettA* (**Extended Data Fig. 1b**). Noticeably, addition of NaCl induced EttA expression as shown using a translational *yfp* (Yellow Fluorescent Protein) reporter fused to *ettA* gene (**Fig. 1b and Extended Data Fig. 1c**).

Proteomic studies were performed on the supernatant (S_{15}) or pellet (P_{150}) fractions from protein extracts from cultures grown in MMAA-NaCl medium, which identified several differences in protein expression in the Δ*ettA* strain compared to the WT or the C_{ettA} strains (**Extended Data Fig. 1d, e**). Coupled with transcriptomic studies on the same cell extracts and

focusing on proteins under-expressed in the Δ*ettA* strain, we identified different scenarios: For *aceB, aceA* and *fumC* genes the corresponding mRNA was expressed at the same level as the WT suggesting a posttranscriptional regulation (**Extended Data Fig. 1f**). For *rraB, yjbJ, elaB,* and *hchA* genes*,* mRNA levels and protein decreased, we hypothesized that the mRNA decay was related to translation because there is an intrinsically close relation between the translation of an mRNA and its stability[53-56]. For other genes, a dominant positive effect on the transcription was observed as, for example, *mgtA*, for which the mechanism of regulation by EttA will be described below. A down-regulation can also be seen for most of the flagella regulon genes, in the Δ*ettA* strain, suggesting a defect in motility in this strain that was validated by motility assays (**Extended Data Fig. 1g, h**).

We confirmed the decrease in expression in the Δ*ettA* strain for five genes (*aceB/A*, *fumC*, *yjbJ* and *hchA*) using a *yfp* reporter where the *yfp* gene, without its initiation codon, was inserted just before the stop codon of the tested genes. The fluorescence level was lower for each construct in the Δ*ettA* strain (**Fig. 1c and Extended Data Fig. 2a**) as well as the protein level quantified by western blot (**Extended Data Fig. 2b**). For *aceB/A* and *fumC* there was no change in their transcription level as determined by northern blot, but for *yjbJ* and *hchA* transcript levels decreased in the Δ*ettA* strain. Other related genes of the metabolic pathway were tested, but they either did not show any change between the strains (*maeB*, *fumB*, *frdB*) or the fluorescence levels were too low to be quantified (*frdA/C/D*, *glcB* and *elaB*) (**Extended Data Fig. 2a**).

Since the phenotype of the Δ*ettA* strain arises when aa, which are primarily metabolized by the TCA cycle[57], are used as carbon source, we tested media with single TCA intermediates as carbon sources. This screen (**Fig. 1c and Extended Data Fig. 1i**) showed that the growth inhibition by salt in the Δ*ettA* strain occurs specifically when malate, fumarate and succinate were used. To our surprise, growth on glyoxylate produced a reversed phenotype where Δ*ettA* grew faster than the other strains.

EttA alleviates ribosome pausing on acidic residues. In a second approach to disengage the five validated *yfp*-reporter fusions from their genomic transcriptional environment, we inserted their sequences from the 5' untranslated region (UTR) of target genes to the *yfp* stop codon in a low copy plasmid (pMMB) under control of an IPTG inducible promoter. The constructs for *aceB*, *fumC*, *hchA* and *yjbJ*, which showed lower expression in the Δ*ettA* strain from their own promoter, also showed lower expression after IPTG induction of the pMMB plasmid in the Δ*ettA* compared to the WT or the C_{ettA} strains, but constructions harboring only the 5'UTR up to the initiation codon of *aceB* or *yjbJ* were expressed independently of EttA (**Extended Data Fig. 3a, b**) showing that the translated sequence is necessary for regulation by EttA.

Next, we made truncations within the target genes in order to determine the minimal sequence that is required for the EttA-dependent expression change (**Fig. 2a and Extended Data Fig. 3a, b**). Constructs with the first 10 or 60 residues of AceB were still subjected to EttA regulation, whereas the construct with only the first eight residues had lost it. The residues absent in this construct, Asp9 and Glu10, are both acidic residues and their replacement by the neutral residues Asn and Gln respectively, also abolished the differential expression in the Δ*ettA* strain. The replacement of one acidic residue reduced the EttA-dependent effect, but two, completely abolished it (**Fig. 2a and Extended Data Fig. 3a, b**). For AceB, the replacement of the three threonines, that precede the acidic residues, by alanine did not affect much the regulation. The gene *aceA* is in an operon after the gene *aceB* and the regulation by EttA was observed only when *aceA:yfp* was expressed as part of the *aceBA* operon, implying a co-translation of the two genes (**Fig. 2a and Extended Data Fig. 3a, b),** the translation of *aceA* being dependent of the rate of translation of *aceB*.

For *fumC*, *yjbJ* and *hchA* genes, the EttA driven regulation was also maintained in constructs that contain at least the first 5-20 N-terminal residues of the encoded protein sequences (FumC: 10 aa, YjbJ: 5 aa and HchA: 20 aa). For these three genes, replacement of two acidic residues (Glu7 Asp9 for FumC, Asp4 Glu5 for YjbJ and Glu15 Asp16 for HchA) by neutral

residues (Asn for Asp and Gln for Glu) abolished the regulation by EttA (**Fig. 2a and Extended Data Fig. 3a and b**). Replacement of only one acidic aa in YjbJ as for AceB reduced the EttA-dependent effect. Overall, these results strongly suggest that EttA can facilitate the translation of mRNA encoding acidic residue repeats at the beginning of their sequence.

In light of these findings, we revisited a subset of our early proteomic targets, some of which we had not previously examined or could not detect the expression with our YFP fusion reporters (**Extended Data Fig. 2a**). We noticed that FrdD, ElaB and RraB contain two or three acidic residues early in their sequences (Asp10 Glu11 for FrdD, Asp11 Asp12 Asp13 for ElaB and Glu8 Glu9 for RraB). We applied the same plasmid-based expression approach to those targets and showed that YFP reporters containing the early part of the target's sequences (FrdD 14 aa, ElaB 15 aa and RraB 10 aa) exhibited a dependency on EttA for their expression. Moreover, the replacement of the acidic residues by neutral ones eliminated the EttA dependency (**Fig. 2a and Extended Data Fig. 3a, b**).

In order to demonstrate the translational regulation driven by EttA, we performed *in vitro* translation assays **(**IVTAs) with mRNA corresponding to the shortest YFP constructs that showed the EttA-dependent differential expression ($aceB_{1\text{-}10aa}$, $yjbJ_{1\text{-}5aa}$ and $rraB_{1\text{-}10aa}$) and with their corresponding mutants that alleviated it ($aceB$-$NQ_{1\text{-}10aa}$, $yjbJ$-$NQ_{1\text{-}5aa}$ and $rraB$-$QQ_{1\text{-}10aa}$). For all the genes, IVTA expression on the WT RNA sequence was increased when some purified and partially monomeric His_6-EttA protein (**Extended Data Fig. 4a**) was added, whereas there was no effect of His_6-EttA on mRNAs where the acidic amino acids had been replaced by neutral residues (**Fig. 2b and Extended Data Fig. 4b**).

To investigate if the acidic residues produce a stalling of the ribosome during translation of the mRNA, we performed some toeprinting assays. Initially we used retapamulin and thiostrepton, two antibiotics which stall ribosomes at start codons, to confirm the translational start site (**Fig. 2c**). The toeprint of the $aceB_{1\text{-}10aa}$ and the $aceB$-$NQ_{1\text{-}10aa}$ constructs were similar in the absence of EttA. The addition of EttA had no effect, but EttA-EQ_2 produced two stalling events.

One at the initiation site on both WT and mutant constructs, consistent with previous results demonstrating that EttA-EQ_2 binds to ribosomes with a free E site, *i.e.* primarily initiating ribosomes[6,7,19,20]. The second stalling event, only present in the *aceB*$_{1\text{-}10aa}$ construct, was identified 24 nt after the initiation toeprinting, which corresponds to the Asp9 codon in the ribosomal P-site. In contrast, *yjbJ* toeprinting (**Fig. 2d**) showed a specific stalling on WT *yjbJ*$_{1\text{-}5aa}$ in addition to the toeprint band of the initiation complex (determined here by toeprinting in presence of EttA-EQ_2 which induced stalling at initiation). This second toeprint signal was not observed when WT EttA was added but was still faintly detected with EttA-EQ_2. This toeprint signal is located 7 nt from the initiation toeprinting, which makes it unclear if the stalling occurred with Lys3 or Asp4 in the P site of the ribosome. We tested if Lys3 had an effect on the regulation by EttA by replacing it by an Ala in our *yjbJ*$_{1\text{-}5aa}$*:yfp* reporter. The related construct showed a similar decrease in expression in the absence of EttA as the WT construct *in vivo*, demonstrating that Lys3 had no impact on the EttA-dependent regulation (**Fig. 2a and Extended Data Fig. 3a**).

Altogether these results argue that polymerization of acidic residues triggers ribosome pausing, leading to two potential outcomes. Firstly, in the case of *aceB*, the absence of a toeprint signal in the absence of EttA, juxtaposed with its presence in the presence of His_6-EttA-EQ_2, strongly suggests ribosome dissociation that can be stabilized by EttA-EQ_2. This possible dissociation is further corroborated by a recent preprint in which the authors show that the introduction of three Glu residues at the beginning of the LacZ protein sequence triggers ribosome dissociation during *in vitro* synthesis, as evidenced by the formation of a peptidyl-tRNA, which can be rescued by EttA[58]. Secondly, for *yjbJ*, a distinct ribosome stalling event is observed, characterized by the detectable toeprinting signal. Notably, EttA is consistently demonstrated as an effective modulator, successfully mitigating ribosomal pausing and thereby augmenting protein expression in all instances. These observations are in agreement with recent reports showing that repeated acidic residues can lead to intrinsic ribosome destabilization[2,3].

Regulation of AceA and AceB expression by EttA explains most observed phenotypes. Three of the proteins for which the synthesis is directly regulated by EttA: AceB (malate synthase), FumC (fumarase C) and FrdD (fumarate reductase subunit D), are enzymes of TCA and glyoxylate shunt pathways. More specifically, they catalyze reactions that use the substrates for which we identified a growth phenotype for the Δ*ettA* strain (**Fig. 1c**). A fourth enzyme, AceA (isocitrate lyase) is indirectly regulated by EttA through the regulation of *aceB*, the upstream gene of the operon (**Fig. 2a**). AceA catalyzes the conversion of isocitrate into succinate and glyoxylate while AceB catalyzes the conversion of glyoxylate and acetyl-CoA into malate and CoA. Together they form the glyoxylate shunt, a metabolic pathway found in some bacteria and plants that bypasses the carbon dioxide-producing steps of the TCA cycle (**Fig. 1c**).

However in *E. coli* the major route to metabolize glyoxylate, is not by converting it to malate by AceB, but by using glyoxylate carboligase[59-62] (Gcl) to condense two glyoxylates into tartronate semialdehyde, which is incorporated into the glycolysis pathway by its conversion to glycerate and then to 2-phosphoglycerate [63,64] (**Fig. 3a**). Accordingly, a deletion of the *gcl* gene is expected to have a drastic effect on *E. coli* growth on glyoxylate and indeed abolished the growth of the three strains on MM with this carbon source (**Fig. 3a and Extended Data Fig. 5a**). We hypothesized that the repression of AceB expression (35% less in Δ*ettA* strain) would promote the metabolic flux toward the *gcl* pathway, thus increasing the growth of the Δ*ettA* strain on glyoxylate (**Fig. 3b**). If so, deletion of *aceB* should increase growth on glyoxylate for all the strains and over-expression should produce the reverse effect. This prediction was confirmed experimentally, where the deletion of *aceB* increased the growth and all the strains grew at the same rate (**Fig. 3a and Extended Data Fig. 5a**). Over-expression of *aceB* reduced the growth rate for all the strains, but the Δ*ettA* strain retained a small advantage of growth. Over-expression of the AceB-NQ variant, for which EttA had no effect on its expression (**Fig. 2a**), also reduced the growth rate of all the strains, but equally in all three strains (**Fig. 3a and Extended Data Fig. 5a**), as expected if the phenotype was due to the regulation of AceB by EttA. The deletion of the second malate

synthase gene (*glcB*), which is expressed at low level in our experimental conditions (**Extended Data Fig. 2a**), also improved growth of all the strains on glyoxylate, but the Δ*ettA* strain maintained a small advantage (**Fig. 3a and Extended Data Fig. 5a**). As expected, the deletion of *aceA* gene had no effect on this phenotype.

To understand the metabolic problem caused by the loss of EttA we tested growth of the strains deleted for genes encoding TCA enzymes in MMAA NaCl. First, deletion of *aceA* had no effect on growth in MMAA medium, but addition of NaCl at 0.4 M prevented the growth of the three strains, suggesting that *aceA* is essential for salt stress in this condition (**Fig. 3a and Extended Data Fig. 5b, c**). The glyoxylate shunt has been previously identified for its importance in tolerance to desiccation[65] and, in plants, to salt[66]. Overall, the results suggest that during salt stress, the Δ*ettA* strain uses less the glyoxylate shunt pathway and therefore probably funnels more metabolic flux through the TCA cycle (**Fig. 3c**). Accordingly, a deletion of the *icd* gene (isocitrate dehydrogenase), which prevents the metabolic flux through the carbon dioxide-producing steps of the TCA cycle, increased the salt sensibility of the Δ*ettA* strain as did the deletion of *fumC* and *frdD* (**Fig. 3a and Extended Data Fig. 5b**). Deletion of *aceB* did not affect the growth phenotype, while overexpression of *aceA* reduced the phenotype (**Fig. 3 and Extended Data Fig. 5b**). This supports the idea that the Δ*ettA* strain defect is partly due to the lower expression of *aceA*. Finally, deletion of *gcl* severely inhibited the growth of the WT and C_{ettA} strains in presence of NaCl, suggesting that they use the conversion of glyoxylate to tartronate semialdehyde in the high salt condition more than the Δ*ettA* strain (without salt, the deletion had no effect on the growth) (**Fig. 3a and Extended Data Fig. 5b**). This observation is also in agreement with the Δ*ettA* strain using principally the TCA cycle and the WT using more the glyoxylate to tartronate semialdehyde pathway. This could be beneficial under salt stress because it could reduce respiration by funneling the metabolic flux towards mixed acid fermentation and/or by increasing synthesis of osmoprotectants by the gluconeogenesis pathway (**Fig. 3c**).

Change of mgtA expression is due to the action of EttA on the translation of the leader peptide MgtL. The proteomic study on the P_{150} protein extracts, which included membrane proteins, showed a 3-fold increase in the Δ*ettA* strain of the protein MgtA, an ATP-dependent Mg^{2+} importer[67]. The expression of the gene *mgtA* is under the regulation of the leader peptide MgtL[3,68,69]. During cellular growth in conditions where Mg^{2+} is not limited, translation of *mgtL* by the ribosome maintains a Rho-dependent terminator (RDT)[3,68,69] accessible to terminate the transcription of the mRNA and therefore prevents the transcription of *mgtA* (**Fig. 4a)**. When Mg^{2+} becomes limiting, the low intracellular concentration favors ribosome dissociation during the translation of *mgtL*. This ribosomal drop-off occurs during the translation of the destabilizing motif EPDP and leads to a conformational change of the mRNA that prevents accessibility to the RDT and transcription termination[3], therefore *mgtA* is transcribed (**Fig. 4a)**. To test if EttA could modulate the translation of *mgtL* and consequently the transcription of *mgtA,* we constructed two reporters using the same plasmid, one with the sequence of *mgtL* (from the 5'UTR to the codon before the stop codon) fused to the *yfp* and the other one from the same 5'UTR extended to the 5th codon of *mgtA* fused to the *yfp* (**Fig. 4b and Extended Data Fig. 6a)**. When strains were grown in the MMAA medium with 2 mM or 0.05 mM of Mg^{2+}, the fluorescence signal was lower in the Δ*ettA* strain for the *mgtL* fusion and higher for the $mgtA_{1\text{-}5aa}$ fusion, in accordance with an action of EttA on the leader peptide MgtL. Also, we showed by northern blot that $mgtA_{1\text{-}5aa}$ transcript increased in the Δ*ettA* strain (**Extended Data Fig. 6c**), consistent with the previously reported transcription termination regulation driven by *mgtL* translation[3,69]. Replacing Glu2 and Asp4 of MgtL with Gln and Asn, respectively, resulted in an increased expression of MgtL fusion in the Δ*ettA* strain to reach the same expression as the WT strain, while MgtA fusion showed no detectable expression, as expected (**Fig. 4b and Extended Data Fig. 6a, b)**.

We used IVTA to determine if EttA directly regulated *mgtL* expression (**Fig. 4c and Extended Data Fig. 6d**) and confirmed that *mgtL* expression was increased in the presence of EttA, but not for the *mgtL* variant where the acidic residues were replaced. Toeprinting performed

on the same constructs showed a toeprint signal, corresponding to a ribosome stalled with Pro3 in the ribosomal P-site in the presence of His_6-EttA, which is even more pronounced in the presence of His_6-EttA-EQ_2. This toeprint signal occurred only for the WT *mgtL* construct (**Fig. 4d**). These observations suggest that EttA can stabilize the ribosome to prevent the drop-off and therefore repress *mgtA* transcription.

The acidic residues need to be within the 30 first aa of the sequence for protein synthesis to be EttA-dependent. We have identified eight proteins for which the synthesis is dependent on EttA and for all of them acidic residues are necessary for this effect. Consequently, we aimed to create a consensus motif derived from these eight sequences, which includes the acidic residues and a few neighboring ones. The consensus sequence NKDEPD, is not naturally found in the *E. coli* proteome. We inserted this consensus sequence after the initiating methionine of the YFP sequence in two different constructs: one with the 5'UTR of *aceB* and the other one with the 5'UTR of *yjbJ*. Both constructs exhibited a strong EttA dependency on expression (**Fig. 5a and Extended Data Fig. 7a, b),** confirming that we can design an artificial sequence that relies on EttA for optimal expression. By reproducing the effect *in vitro* in an IVTA using the 5'UTR *aceB* construct, we confirmed that this occurred by direct interaction of EttA on the translating ribosome (**Fig. 5b and Extended Data Fig. 7c**). We tested a construct that expressed the same aa sequence but used different synonymous codons (syn-codons). This construct had a drop in the overall expression level, but the EttA dependency on expression was maintained, therefore the EttA regulatory effect is dependent on the aa, but not on the codons used (**Fig. 5a and Extended Data Fig. 7a, b**).

To determine if the position of this sequence had an importance for the EttA-dependent expression, we tested several constructs where this sequence was moved by increments of 10 aa away from the initiating methionine. We used the sequence of AceB-NQ, whose expression is no longer EttA-dependent, to test the 10 aa increments. Displaced by 10 aa, the consensus sequence

still produced a strong induction by EttA. When displaced by 20 aa, there was only a small, not statistically significant, induction by EttA, while at 30 and 40 aa there was no effect of EttA (**Fig. 5a and Extended Data Fig. 7a, b)**. This experiment demonstrated that the acidic residues need to be within the first 30 aa of a protein sequence to make its expression EttA-dependent.

Since we found that two acid residues in the beginning of the sequence can make protein synthesis dependent on EttA, we wondered if it could be detected genome-wide in our proteomic studies. We searched for the presence of a motif where two acidic residues are adjacent or separated by one aa in the first 50 aa of *E. coli* proteome (Motif: -/$X_{0,1}$/-). Then we grouped them according to the position of the acidic residues within segments of 10 aa and compared the ratio of expression of the WT versus the Δ*ettA* or C_{ettA} strains (**Fig. 5c and Extended Data Fig. 7d**). This analysis revealed that the presence of the motif within the first 20 aa correlated with a statistically significant decrease of expression only in the Δ*ettA* strain and with a stronger effect when it is located within the first 10 aa.

The analysis of the proteomic data also revealed that certain proteins containing double acidic residues early in their sequences remain unaffected by *ettA* deletion. Furthermore, the YFP sequence begins with "MVSKGEE" and its expression remains unaffected by EttA (**Extended Data Fig. 7e, f**). We attempted to render YFP expression dependent on EttA by introducing sequential mutations in the acidic residues and their surroundings (**Extended Data Fig. 7e, f**). Neither the EE nor DE motif alone led to EttA dependency. Even though the ED motif showed a statistically significant change, it was only around 7%, which is less than changes observed with EttA's physiological targets. In fact, at a minimum, a DPEE motif was necessary. The presence of a Pro suggests that a structural constraint on the positioning of the nascent peptide is crucial for this phenomenon to occur.

DISCUSSION

We have demonstrated that EttA enhances translation of specific mRNA (*aceB*, *rraB*, *yjbJ*,

fumC, frdD, hchA, *elaB* and *mgtL*). This specificity arises from the destabilizing effect of early acidic residues during protein synthesis, which EttA mitigates. According to our proposed model (**Fig. 5d**), EttA initially binds to a ribosome that has paused at the acidic residues, most likely before the peptide bond formation of the second acidic residue occurs (**Fig. 2c, d and Fig. 4d**). In this state, it can avert ribosome dissociation, as exemplified by *aceB,* and *mgtL* (**Fig. 2c, Fig. 4d**), where the toeprinting didn't detect stalling in the absence of His_6-EttA, but did detect stalling with His_6-EttA-EQ_2, suggesting that the non-hydrolytic EttA mutant can prevent the ribosome dissociation but cannot restore the elongation. In the case of *yjbJ*, the initial pausing does not lead to ribosomal drop-off since a clear stalling signal is seen on the toeprinting experiments in the absence of EttA (**Fig. 2d**). In the final step, EttA allows the elongation to restart. Ribosomal dissociation during elongation of acidic-residues has been previously demonstrated for MgtL and other proteins in prokaryotes[2,3] and eukaryotes[1], this effect was described as Intrinsic Ribosome Destabilization (IRD). Moreover, a recent report suggest that EttA can prevent the IRD *in vitro*[58].

This model draws parallels with the function of the translation factor EF-P[70], which enhances translation of polyproline-containing proteins[29,30]. Polyproline-containing nascent chains adopt a conformation that is incompatible with the ribosome's NPET structure, creating tension on the peptidyl-tRNA[71] that prevents the formation of the peptide bond with the Pro-tRNA in the A site. EF-P binding to the stalled ribosome forces the polyproline-containing nascent chain to adopt a correct conformation. While the structures of EF-P and EttA differ significantly (**Extended Data Fig. 8a**), comparative analysis of their ribosome complexes[23,71] aligned on domain V of 23S rRNA, highlights the close proximity of the loop in EF-P's extension containing the essential β-lysyl-lysine residue and the loop in EttA's PtIM, with distances ranging from 1.9 to 3 Å (**Fig. 5e and Extended Data Fig. 8b**).

These structural and functional similarities occur in the region of the proteins that interact with the acceptor stem of the P-site tRNA. Furthermore, the structures of EttA-EQ_2 in complex with initiating or elongating ribosomes[23] indicate that the geometry of the P-site tRNA is

conducive to peptide bond formation, akin to the structures observed in EF-P ribosomal complexes[71]. Additionally, a recent preprint described in *Bacillus subtilis* a an ABC-F protein that can partially overlap with the function of EF-P[72].

The stalling caused by polyproline is context-dependent, depending on the position within the sequence and on the sequence context[73,74]. Similarly, the stalling induced by acidic residues, rescued by EttA, is not universal. Although we have shown EttA's influence on several proteins with acidic residue repeats within the first 30 amino acids (**Fig. 2, Fig. 4b and Fig. 5a**), we have also identified other proteins with this feature that do not rely on EttA for their expression (**Fig. 5c**). Therefore, the mere presence of di-acidic residues is insufficient to destabilize translating ribosomes and render translation EttA-dependent. The conformation of the nascent peptide in the ribosome's NPET appears to be crucial, with the presence of a proline upstream of the acidic residues in four of our eight targets supporting this notion. However, fundamental differences exist between EF-P and EttA. In the case of polyproline, stalling can occur after the nascent peptide has filled the entire ribosomal NPET[29,30,73,74]. In contrast, the stalling induced by acidic residues, rescued by EttA, is limited to a partially filled NPET. EF-P functions by binding to the stalled complex and by inducing rescue[71], while EttA, employs its ATPase activity following binding, to potentially reshape the nascent peptide's positioning within the NPET/PTC [23].

ARE ABC-F proteins provide resistance against antibiotics that target the PTC and the NPET[10,14-20]. Many of these antibiotics exhibit context-dependent action, meaning the nascent peptide's sequence influences their efficacy[4,5,75,76]. Therefore, the sequence of amino acids in the NPET holds significance, paralleling the concept presented here. Despite the absence of an inducer (antibiotic) in EttA's case, this suggests that the actions of ARE ABC-F and ABC-F on the ribosome share similarities and may have evolved from a common rescue mechanism.

Our study reveals that EttA directly influences three genes (*aceB*, *frdD*, *fumC*) and indirectly affects *aceA*, all functionally interconnected within the TCA and glyoxylate shunt pathways (**Fig. 1a**). This highlights EttA's role in coordinating key metabolic pathways by

governing the expression of functionally related genes. Importantly, the malate synthase AceB retains its function when the acidic residues are mutated in the AceB-NQ construct. However, its expression is no longer dependent on EttA, implying that these residues can act as a regulatory signal (**Fig. 3a and Extended Data Fig. 5a**). Additional EttA-dependent genes exhibit functional links. The protein/nucleic acid deglycase 1 (HchA) repairs glyoxal- and methylglyoxal-glycated proteins as well as nucleotides[77,78] by releasing glycolate or lactate from the modified amino acid or nucleotide. The glycolate can be converted into glyoxylate by the Glycolate dehydrogenase (GlcDEF)[79] and will benefit from the EttA-dependent expression of *aceB* for its degradation. The function of the protein YjbJ is unknown, but its expression is abundant during the stationary phase and salt stress[80,81] as is the membrane protein, ElaB, which has been associated with resistance to multiple stresses[82]. The protein RraB modulates RNase E (the main RNase of *E. coli)* activity[83-85], adding another layer of regulation by EttA. MgtA is an ATP-dependent Mg^{2+} importer[67] expressed when cells are deprived of Mg^{2+}, its expression regulated by EttA through the leader peptide MgtL, assists in Mg^{2+} homeostasis. This example further demonstrates EttA's potential to repress gene expression using a leader peptide, as documented in certain ARE ABC-F cases[18,33].

EttA plays a pivotal role in regulating the interplay between the TCA and glyoxylate shunt pathways through the translational regulation of *aceB*, *fumC*, and *frdD* genes. Reduced expression of these genes, particularly *aceB*, and indirectly *aceA* in the Δ*ettA* strain, results in distinct growth phenotypes by reducing the glyoxylate shunt metabolic flux in favor of the TCA cycle or the tartronate-semialdehyde flux. The Δ*ettA* strain exhibits improved growth when glyoxylate is the sole carbon source but performs worse when amino acids are the only carbon source and when subjected to salt stress (**Fig. 1a, c**). In the MMAA NaCl medium, the WT strain efficiently manages salt stress by redirecting metabolic flux through the glyoxylate and tartronate-semialdehyde pathways (**Fig. 3c**), providing benefits such as increased glycolysis for osmoprotectant production[86,87] (e.g., sucrose and trehalose) and reduced NADH and NADPH production in the TCA carbon dioxide-producing steps. These results support recent studies that have shown the

importance of the glyoxylate shunt in stress conditions[65,66,88-90].

These findings underscore EttA's crucial role in the cellular stress response, as it is induced by high salt (**Fig. 1b**) and is part of the RpoS regulon[91,92]. Moreover, our discovery that EttA primarily governs the expression of genes intricately linked to central metabolism, influencing cellular energy levels, suggests that EttA possesses the ability to adapt gene expression according to the prevailing cellular energy state. This adaptation is related to EttA's established dependence on the ADP:ATP ratio[6,7], providing a direct mechanism to connect its regulatory effects to cellular energy status, which warrants further investigation in future studies.

DATA AVAILABILITY

RNA-sequencing data are available through the EBI ArrayExpress database (https://www.ebi.ac.uk/biostudies/arrayexpress/studies) under accession code: E-MTAB-13458. Proteomic data are available through the massIVE Repository (https://massive.ucsd.edu/ProteoSAFe/static/massive.jsp) under accession code: MSV000093143.

ACKNOWLEDGEMENTS

FO, TO and GB were supported by funds from the CNRS (UMR8261), Université Paris Cité, the LABEX program (DYNAMO ANR-11-LABX-0011), and two ANR grants (EZOtrad/ANR-14-ACHN-0027 and ABC-F_AB/ANR-18-CE35-0010). FO received a fellowship from the Edmond de Rothschild Foundation. This work was also supported by the EQUIPEX CACSICE (ANR-11-EQPX-0008), through funding of the Proteomic Platform of IBPC. We express our great gratitude to Pr. Hirotada Mori for his gifts of the Keio collection and the YFP fusion strains collection. We thank Alexandre Pozza for its help with SEC-MALS

experiments. The authors thank Jackie Plumbridge, Nicolas Biais and John F. Hunt for their advice and help.

AUTHOR CONTRIBUTIONS

FO constructed all the strains, performed most of the experiments, TO and SN performed some bacterial cultures and samples preparations, SN performed the northern-blot experiments, MH performed the proteomic analysis, AON generated early results used for this study. FO, GB and LM analyzed the data and prepared the figures, GB designed the research program. GB, LM and FO wrote the manuscript in consultation with the other authors.

COMPETING FINANCIAL INTERESTS

The authors declare no competing financial interests.

REFERENCES

1 Ito, Y. *et al.* Nascent peptide-induced translation discontinuation in eukaryotes impacts biased amino acid usage in proteomes. *Nat Commun* **13**, 7451 (2022). https://doi.org:10.1038/s41467-022-35156-x

2 Chadani, Y. *et al.* Nascent polypeptide within the exit tunnel stabilizes the ribosome to counteract risky translation. *EMBO J* **40**, e108299 (2021). https://doi.org:10.15252/embj.2021108299

3 Chadani, Y. *et al.* Intrinsic Ribosome Destabilization Underlies Translation and Provides an Organism with a Strategy of Environmental Sensing. *Mol Cell* **68**, 528-539 e525 (2017). https://doi.org:10.1016/j.molcel.2017.10.020

4 Marks, J. *et al.* Context-specific inhibition of translation by ribosomal antibiotics targeting the peptidyl transferase center. *Proc Natl Acad Sci U S A* **113**, 12150-12155 (2016). https://doi.org:10.1073/pnas.1613055113

5 Choi, J. *et al.* Dynamics of the context-specific translation arrest by chloramphenicol and linezolid. *Nature chemical biology* **16**, 310-317 (2020). https://doi.org:10.1038/s41589-019-0423-2

6 Boel, G. *et al.* The ABC-F protein EttA gates ribosome entry into the translation elongation cycle. *Nat Struct Mol Biol* **21**, 143-151 (2014). https://doi.org:10.1038/nsmb.2740

7 Chen, B. *et al.* EttA regulates translation by binding the ribosomal E site and restricting ribosome-tRNA dynamics. *Nat Struct Mol Biol* **21**, 152-159 (2014). https://doi.org:10.1038/nsmb.2741

8 Davidson, A. L., Dassa, E., Orelle, C. & Chen, J. Structure, function, and evolution of bacterial ATP-binding cassette systems. *Microbiology and molecular biology reviews : MMBR* **72**, 317-364, table of contents (2008). https://doi.org:10.1128/MMBR.00031-07

9 Sharkey, L. K., Edwards, T. A. & O'Neill, A. J. ABC-F Proteins Mediate Antibiotic Resistance through Ribosomal Protection. *mBio* **7**, e01975 (2016). https://doi.org:10.1128/mBio.01975-15

10 Crowe-McAuliffe, C. *et al.* Structural basis for antibiotic resistance mediated by the Bacillus subtilis ABCF ATPase VmlR. *Proc Natl Acad Sci U S A* **115**, 8978-8983 (2018). https://doi.org:10.1073/pnas.1808535115

11 Murina, V., Kasari, M., Hauryliuk, V. & Atkinson, G. C. Antibiotic resistance ABCF proteins reset the peptidyl transferase centre of the ribosome to counter translational arrest. *Nucleic Acids Res* **46**, 3753-3763 (2018). https://doi.org:10.1093/nar/gky050

12 Su, W. *et al.* Ribosome protection by antibiotic resistance ATP-binding cassette protein. *Proc Natl Acad Sci U S A* **115**, 5157-5162 (2018). https://doi.org:10.1073/pnas.1803313115

13 Murina, V. *et al.* ABCF ATPases Involved in Protein Synthesis, Ribosome Assembly and Antibiotic Resistance: Structural and Functional Diversification across the Tree of Life. *J Mol Biol* **431**, 3568-3590 (2019). https://doi.org:10.1016/j.jmb.2018.12.013

14 Lenart, J., Vimberg, V., Vesela, L., Janata, J. & Balikova Novotna, G. Detailed mutational analysis of Vga(A) interdomain linker: implication for antibiotic resistance specificity and mechanism. *Antimicrob Agents Chemother* **59**, 1360-1364 (2015). https://doi.org:10.1128/AAC.04468-14

15 Vimberg, V. *et al.* Ribosome-Mediated Attenuation of vga(A) Expression Is Shaped by the Antibiotic Resistance Specificity of Vga(A) Protein Variants. *Antimicrob Agents Chemother* **64** (2020). https://doi.org:10.1128/AAC.00666-20

16 Obana, N. *et al.* Genome-encoded ABCF factors implicated in intrinsic antibiotic resistance in Gram-positive bacteria: VmlR2, Ard1 and CplR. *Nucleic Acids Res* **51**, 4536-4554 (2023). https://doi.org:10.1093/nar/gkad193

17 Mohamad, M. *et al.* Sal-type ABC-F proteins: intrinsic and common mediators of pleuromutilin resistance by target protection in staphylococci. *Nucleic Acids Res* **50**, 2128-2142 (2022). https://doi.org:10.1093/nar/gkac058

18 Koberska, M. *et al.* Beyond Self-Resistance: ABCF ATPase LmrC Is a Signal-Transducing Component of an Antibiotic-Driven Signaling Cascade Accelerating the Onset of Lincomycin Biosynthesis. *mBio* **12**, e0173121 (2021). https://doi.org:10.1128/mBio.01731-21

19 Crowe-McAuliffe, C. *et al.* Structural basis of ABCF-mediated resistance to pleuromutilin, lincosamide, and streptogramin A antibiotics in Gram-positive pathogens. *Nat Commun* **12**, 3577 (2021). https://doi.org:10.1038/s41467-021-23753-1

20 Crowe-McAuliffe, C. *et al.* Structural basis for PoxtA-mediated resistance to phenicol and oxazolidinone antibiotics. *Nat Commun* **13**, 1860 (2022). https://doi.org:10.1038/s41467-022-29274-9

21 Ousalem, F., Singh, S., Chesneau, O., Hunt, J. F. & Boel, G. ABC-F proteins in mRNA translation and antibiotic resistance. *Research in microbiology* **170**, 435-447 (2019). https://doi.org:10.1016/j.resmic.2019.09.005

22 Ousalem, F. *et al.* Comparative genetic, biochemical, and biophysical analyses of the four *E. coli* ABCF paralogs support distinct functions related to mRNA translation. *bioRxiv*, 2023.2006.2011.543863 (2023). https://doi.org:10.1101/2023.06.11.543863

23 Singh, S. *et al.* Cryo-EM studies of the four *E. coli* paralogs establish ABCF proteins as master plumbers of the peptidyl-transferase center of the ribosome. *bioRxiv*, 2023.2006.2015.543498 (2023). https://doi.org:10.1101/2023.06.15.543498

24 Fostier, C. R. *et al.* ABC-F translation factors: from antibiotic resistance to immune response. *FEBS Lett* **595**, 675-706 (2021). https://doi.org:10.1002/1873-3468.13984

25 Punta, M. *et al.* The Pfam protein families database. *Nucleic Acids Res* **40**, D290-301 (2012). https://doi.org:10.1093/nar/gkr1065

26 Smith, P. C. *et al.* ATP binding to the motor domain from an ABC transporter drives formation of a nucleotide sandwich dimer. *Mol Cell* **10**, 139-149 (2002). https://doi.org:10.1016/s1097-2765(02)00576-2

27 Cui, Z. *et al.* Interplay between an ATP-binding cassette F protein and the ribosome from Mycobacterium tuberculosis. *Nat Commun* **13**, 432 (2022). https://doi.org:10.1038/s41467-022-28078-1

28 Su, T. *et al.* Structure and function of Vms1 and Arb1 in RQC and mitochondrial proteome homeostasis. *Nature* **570**, 538-542 (2019). https://doi.org:10.1038/s41586-019-1307-z

29 Doerfel, L. K. *et al.* EF-P is essential for rapid synthesis of proteins containing consecutive proline residues. *Science* **339**, 85-88 (2013). https://doi.org:10.1126/science.1229017

30 Ude, S. *et al.* Translation elongation factor EF-P alleviates ribosome stalling at polyproline stretches. *Science* **339**, 82-85 (2013). https://doi.org:10.1126/science.1228985

31 Gutierrez, E. *et al.* eIF5A promotes translation of polyproline motifs. *Mol Cell* **51**, 35-45 (2013). https://doi.org:10.1016/j.molcel.2013.04.021

32 Murina, V., Kasari, M., Hauryliuk, V. & Atkinson, G. C. Antibiotic resistance ABCF proteins reset the peptidyl transferase centre of the ribosome to counter translational arrest. *Nucleic Acids Res*, gky050-gky050 (2018). https://doi.org:10.1093/nar/gky050

33 Fostier, C. R. *et al.* Regulation of the macrolide resistance ABC-F translation factor MsrD. *Nature Communications* **14**, 3891 (2023). https://doi.org:10.1038/s41467-023-39553-8

34 Vazquez de Aldana, C. R., Marton, M. J. & Hinnebusch, A. G. GCN20, a novel ATP binding cassette protein, and GCN1 reside in a complex that mediates activation of the eIF-2 alpha kinase GCN2 in amino acid-starved cells. *The EMBO journal* **14**, 3184-3199 (1995).

35 Sattlegger, E. & Hinnebusch, A. G. Polyribosome binding by GCN1 is required for full activation of eukaryotic translation initiation factor 2{alpha} kinase GCN2 during amino acid starvation. *J Biol Chem* **280**, 16514-16521 (2005). https://doi.org:10.1074/jbc.M414566200

36 Dong, J., Lai, R., Jennings, J. L., Link, A. J. & Hinnebusch, A. G. The novel ATP-binding cassette protein ARB1 is a shuttling factor that stimulates 40S and 60S ribosome biogenesis. *Mol Cell Biol* **25**, 9859-9873 (2005). https://doi.org:10.1128/MCB.25.22.9859-9873.2005

37 Paytubi, S. *et al.* ABC50 promotes translation initiation in mammalian cells. *J Biol Chem* **284**, 24061-24073 (2009). https://doi.org:10.1074/jbc.M109.031625

38 Arora, H. *et al.* The ATP-Binding Cassette Gene ABCF1 Functions as an E2 Ubiquitin-Conjugating Enzyme Controlling Macrophage Polarization to Dampen Lethal Septic Shock. *Immunity* **50**, 418-431 e416 (2019). https://doi.org:10.1016/j.immuni.2019.01.014

39 Richard, M., Drouin, R. & Beaulieu, A. D. ABC50, a novel human ATP-binding cassette protein found in tumor necrosis factor-alpha-stimulated synoviocytes. *Genomics* **53**, 137-145 (1998). https://doi.org:10.1006/geno.1998.5480

40 Semov, A. *et al.* Alterations in TNF- and IL-related gene expression in space-flown WI38 human fibroblasts. *FASEB J* **16**, 899-901 (2002). https://doi.org:10.1096/fj.01-1002fje

41 Yu, Y., Zhang, Y., Zhu, Z. & Berger, S. A. ABC50 modulates sensitivity of HL60 leukemic cells to endoplasmic reticulum (ER) stress-induced cell death. *Biochem Pharmacol* **81**, 488-497 (2011). https://doi.org:10.1016/j.bcp.2010.11.007

42 Setia, N., Abbas, O., Sousa, Y., Garb, J. L. & Mahalingam, M. Profiling of ABC transporters ABCB5, ABCF2 and nestin-positive stem cells in nevi, in situ and invasive melanoma. *Modern pathology : an official journal of the United States and Canadian Academy of Pathology, Inc* **25**, 1169-1175 (2012). https://doi.org:10.1038/modpathol.2012.71

43 Verma, N., Ahuja, V. & Paul, J. Profiling of ABC transporters during active ulcerative colitis and in vitro effect of inflammatory modulators. *Digestive diseases and sciences* **58**, 2282-2292 (2013). https://doi.org:10.1007/s10620-013-2636-7

44 Lee, M. N. *et al.* Identification of regulators of the innate immune response to cytosolic DNA and retroviral infection by an integrative approach. *Nat Immunol* **14**, 179-185 (2013). https://doi.org:10.1038/ni.2509

45 Boonstra, R. *et al.* Mitoxantrone resistance in a small cell lung cancer cell line is associated with ABCA2 upregulation. *British journal of cancer* **90**, 2411-2417 (2004). https://doi.org:10.1038/sj.bjc.6601863

46 Ogawa, Y. *et al.* Clinical role of ABCF2 expression in breast cancer. *Anticancer research* **26**, 1809-1814 (2006).

47 Hendig, D. *et al.* Characterization of the ATP-binding cassette transporter gene expression profile in Y79: a retinoblastoma cell line. *Mol Cell Biochem* **328**, 85-92 (2009). https://doi.org:10.1007/s11010-009-0077-6

48 Cunha, I. W. *et al.* Identification of genes associated with local aggressiveness and metastatic behavior in soft tissue tumors. *Transl Oncol* **3**, 23-32 (2010). https://doi.org:10.1593/tlo.09166

49 Hlavata, I. *et al.* The role of ABC transporters in progression and clinical outcome of colorectal cancer. *Mutagenesis* **27**, 187-196 (2012). https://doi.org:10.1093/mutage/ger075

50 Hlavac, V. *et al.* The expression profile of ATP-binding cassette transporter genes in breast carcinoma. *Pharmacogenomics* **14**, 515-529 (2013). https://doi.org:10.2217/pgs.13.26

51 Antonova, O. *et al.* Changes in the gene expression profile of the bladder cancer cell lines after treatment with Helix lucorum and Rapana venosa hemocyanin. *J BUON* **20**, 180-187 (2015).

52 Li, X. *et al.* Elevated microRNA-23a Expression Enhances the Chemoresistance of Colorectal Cancer Cells with Microsatellite Instability to 5-Fluorouracil by Directly Targeting ABCF1. *Curr Protein Pept Sci* **16**, 301-309 (2015). https://doi.org:10.2174/1389203716041504291533 09

53 Boel, G. *et al.* Codon influence on protein expression in E. coli correlates with mRNA levels. *Nature* **529**, 358-363 (2016). https://doi.org:10.1038/nature16509

54 Presnyak, V. *et al.* Codon optimality is a major determinant of mRNA stability. *Cell* **160**, 1111-1124 (2015). https://doi.org:10.1016/j.cell.2015.02.029

55 Bazzini, A. A. *et al.* Codon identity regulates mRNA stability and translation efficiency during the maternal-to-zygotic transition. *EMBO J* **35**, 2087-2103 (2016). https://doi.org:10.15252/embj.201694699

56 Mishima, Y. & Tomari, Y. Codon Usage and 3' UTR Length Determine Maternal mRNA Stability in Zebrafish. *Mol Cell* **61**, 874-885 (2016). https://doi.org:10.1016/j.molcel.2016.02.027

57 Zampieri, M., Horl, M., Hotz, F., Muller, N. F. & Sauer, U. Regulatory mechanisms underlying coordination of amino acid and glucose catabolism in Escherichia coli. *Nat Commun* **10**, 3354 (2019). https://doi.org:10.1038/s41467-019-11331-5

58 Chadani, Y., Uemura, E., Yamazaki, K., Kurihara, M. & Taguchi, H. The ABCF proteins in Escherichia coli individually alleviate nascent peptide-induced noncanonical translations. *bioRxiv*, 2023.2010.2004.560807 (2023). https://doi.org:10.1101/2023.10.04.560807

59 Kaplun, A. *et al.* Glyoxylate carboligase lacks the canonical active site glutamate of thiamine-dependent enzymes. *Nature chemical biology* **4**, 113-118 (2008). https://doi.org:10.1038/nchembio.62

60 Gupta, N. K. & Vennesland, B. Glyoxylate Carboligase of Escherichia Coli: A Flavoprotein. *The Journal of biological chemistry* **239**, 3787-3789 (1964).

61 Chang, Y. Y., Wang, A. Y. & Cronan, J. E., Jr. Molecular cloning, DNA sequencing, and biochemical analyses of Escherichia coli glyoxylate carboligase. An enzyme of the acetohydroxy acid synthase-pyruvate oxidase family. *The Journal of biological chemistry* **268**, 3911-3919 (1993).

62 Ornston, L. N. & Ornston, M. K. Regulation of glyoxylate metabolism in Escherichia coli K-12. *Journal of bacteriology* **98**, 1098-1108 (1969). https://doi.org:10.1128/jb.98.3.1098-1108.1969

63 Karp, P. D. *et al.* The EcoCyc Database. *EcoSal Plus* **8** (2018). https://doi.org:10.1128/ecosalplus.ESP-0006-2018

64 Zelcbuch, L. *et al.* An in vivo metabolic approach for deciphering the product specificity of glycerate kinase proves that both E. coli's glycerate kinases generate 2-phosphoglycerate. *PloS one* **10**, e0122957 (2015). https://doi.org:10.1371/journal.pone.0122957

65 Erkut, C., Gade, V. R., Laxman, S. & Kurzchalia, T. V. The glyoxylate shunt is essential for desiccation tolerance in C. elegans and budding yeast. *Elife* **5**, e13614 (2016). https://doi.org:10.7554/eLife.13614

66 Yuenyong, W., Sirikantaramas, S., Qu, L. J. & Buaboocha, T. Isocitrate lyase plays important roles in plant salt tolerance. *BMC Plant Biol* **19**, 472 (2019). https://doi.org:10.1186/s12870-019-2086-2

67 Smith, R. L. & Maguire, M. E. Microbial magnesium transport: unusual transporters searching for identity. *Mol Microbiol* **28**, 217-226 (1998). https://doi.org:10.1046/j.1365-2958.1998.00810.x

68 Zhao, G., Kong, W., Weatherspoon-Griffin, N., Clark-Curtiss, J. & Shi, Y. Mg2+ facilitates leader peptide translation to induce riboswitch-mediated transcription termination. *EMBO J* **30**, 1485-1496 (2011). https://doi.org:10.1038/emboj.2011.66

69 Gall, A. R. *et al.* Mg2+ regulates transcription of mgtA in Salmonella Typhimurium via translation of proline codons during synthesis of the MgtL peptide. *Proc Natl Acad Sci U S A* **113**, 15096-15101 (2016). https://doi.org:10.1073/pnas.1612268113

70 Glick, B. R. & Ganoza, M. C. Identification of a soluble protein that stimulates peptide bond synthesis. *Proc Natl Acad Sci U S A* **72**, 4257-4260 (1975). https://doi.org:10.1073/pnas.72.11.4257

71 Huter, P. *et al.* Structural Basis for Polyproline-Mediated Ribosome Stalling and Rescue by the Translation Elongation Factor EF-P. *Mol Cell* **68**, 515-527 e516 (2017). https://doi.org:10.1016/j.molcel.2017.10.014

72 Hong, H.-R., Prince, C. R., Wu, L. & Feaga, H. A. Identification of factors that prevent ribosome stalling during early elongation. *bioRxiv*, 2023.2008.2004.552005 (2023). https://doi.org:10.1101/2023.08.04.552005

73 Woolstenhulme, C. J., Guydosh, N. R., Green, R. & Buskirk, A. R. High-precision analysis of translational pausing by ribosome profiling in bacteria lacking EFP. *Cell Rep* **11**, 13-21 (2015). https://doi.org:10.1016/j.celrep.2015.03.014

74 Starosta, A. L. *et al.* Translational stalling at polyproline stretches is modulated by the sequence context upstream of the stall site. *Nucleic Acids Res* **42**, 10711-10719 (2014). https://doi.org:10.1093/nar/gku768

75 Beckert, B. *et al.* Structural and mechanistic basis for translation inhibition by macrolide and ketolide antibiotics. *Nat Commun* **12**, 4466 (2021). https://doi.org:10.1038/s41467-021-24674-9

76 Kannan, K. *et al.* The general mode of translation inhibition by macrolide antibiotics. *Proc Natl Acad Sci U S A* **111**, 15958-15963 (2014). https://doi.org:10.1073/pnas.1417334111

77 Richarme, G. *et al.* Guanine glycation repair by DJ-1/Park7 and its bacterial homologs. *Science* **357**, 208-211 (2017). https://doi.org:10.1126/science.aag1095

78 Richarme, G. *et al.* Parkinsonism-associated protein DJ-1/Park7 is a major protein deglycase that repairs methylglyoxal- and glyoxal-glycated cysteine, arginine, and lysine residues. *The Journal of biological chemistry* **290**, 1885-1897 (2015). https://doi.org:10.1074/jbc.M114.597815

79 Pellicer, M. T., Badia, J., Aguilar, J. & Baldoma, L. glc locus of Escherichia coli: characterization of genes encoding the subunits of glycolate oxidase and the glc regulator protein. *Journal of bacteriology* **178**, 2051-2059 (1996). https://doi.org:10.1128/jb.178.7.2051-2059.1996

80 Weber, H., Polen, T., Heuveling, J., Wendisch, V. F. & Hengge, R. Genome-wide analysis of the general stress response network in Escherichia coli: sigmaS-dependent genes, promoters, and sigma factor selectivity. *Journal of bacteriology* **187**, 1591-1603 (2005). https://doi.org:10.1128/JB.187.5.1591-1603.2005

81 Weber, A., Kogl, S. A. & Jung, K. Time-dependent proteome alterations under osmotic stress during aerobic and anaerobic growth in Escherichia coli. *Journal of bacteriology* **188**, 7165-7175 (2006). https://doi.org:10.1128/JB.00508-06

82 Guo, Y. *et al.* Tail-Anchored Inner Membrane Protein ElaB Increases Resistance to Stress While Reducing Persistence in Escherichia coli. *Journal of bacteriology* **199** (2017). https://doi.org:10.1128/JB.00057-17

83 Lee, K. *et al.* RraA. *Cell* **114**, 623-634 (2003). https://doi.org:10.1016/j.cell.2003.08.003

84 Gao, J. *et al.* Differential modulation of E. coli mRNA abundance by inhibitory proteins that alter the composition of the degradosome. *Mol Microbiol* **61**, 394-406 (2006). https://doi.org:10.1111/j.1365-2958.2006.05246.x

85 Yeom, J. H. *et al.* Inhibitory effects of RraA and RraB on RNAse E-related enzymes imply conserved functions in the regulated enzymatic cleavage of RNA. *FEMS Microbiol Lett* **285**, 10-15 (2008). https://doi.org:10.1111/j.1574-6968.2008.01205.x

86 Gouffi, K. *et al.* Sucrose is a nonaccumulated osmoprotectant in Sinorhizobium meliloti. *Journal of bacteriology* **180**, 5044-5051 (1998). https://doi.org:10.1128/JB.180.19.5044-5051.1998

87 Cayley, S. & Record, M. T., Jr. Roles of cytoplasmic osmolytes, water, and crowding in the response of Escherichia coli to osmotic stress: biophysical basis of osmoprotection by glycine betaine. *Biochemistry* **42**, 12596-12609 (2003). https://doi.org:10.1021/bi0347297

88 Ahn, S., Jung, J., Jang, I. A., Madsen, E. L. & Park, W. Role of Glyoxylate Shunt in Oxidative Stress Response. *The Journal of biological chemistry* **291**, 11928-11938 (2016). https://doi.org:10.1074/jbc.M115.708149

89 Park, C., Shin, B. & Park, W. Alternative fate of glyoxylate during acetate and hexadecane metabolism in Acinetobacter oleivorans DR1. *Sci Rep* **9**, 14402 (2019). https://doi.org:10.1038/s41598-019-50852-3

90 Koedooder, C. *et al.* The Role of the Glyoxylate Shunt in the Acclimation to Iron Limitation in Marine Heterotrophic Bacteria. *Frontiers in Marine Science* **5** (2018). https://doi.org:10.3389/fmars.2018.00435

91 Huerta, A. M. & Collado-Vides, J. Sigma70 promoters in Escherichia coli: specific transcription in dense regions of overlapping promoter-like signals. *J Mol Biol* **333**, 261-278 (2003). https://doi.org:10.1016/j.jmb.2003.07.017

92 Keseler, I. M. *et al.* The EcoCyc Database in 2021. *Front Microbiol* **12**, 711077 (2021). https://doi.org:10.3389/fmicb.2021.711077

93 Blattner, F. R. *et al.* The Complete Genome Sequence of Escherichia coli K-12. *Science* **277**, 1453-1462 (1997). https://doi.org:doi:10.1126/science.277.5331.1453

94 St-Pierre, F. *et al.* One-step cloning and chromosomal integration of DNA. *ACS synthetic biology* **2**, 537-541 (2013). https://doi.org:10.1021/sb400021j

95 Otsuka, Y. *et al.* GenoBase: comprehensive resource database of Escherichia coli K-12. *Nucleic Acids Res* **43**, D606-617 (2015). https://doi.org:10.1093/nar/gku1164

96 Datsenko, K. A. & Wanner, B. L. One-step inactivation of chromosomal genes in Escherichia coli K-12 using PCR products. *Proc Natl Acad Sci U S A* **97**, 6640-6645 (2000). https://doi.org:10.1073/pnas.120163297

97 Baba, T. *et al.* Construction of Escherichia coli K-12 in-frame, single-gene knockout mutants: the Keio collection. *Molecular systems biology* **2**, 2006 0008 (2006). https://doi.org:10.1038/msb4100050

98 Jansson, M. *et al.* High-level production of uniformly (1)(5)N- and (1)(3)C-enriched fusion proteins in Escherichia coli. *Journal of biomolecular NMR* **7**, 131-141 (1996).

99 Stead, M. B. *et al.* RNA snap ™: a rapid, quantitative and inexpensive, method for isolating total RNA from bacteria. *Nucleic Acids Research* **40**, e156-e156 (2012). https://doi.org:10.1093/nar/gks680

100 Langmead, B. & Salzberg, S. L. Fast gapped-read alignment with Bowtie 2. *Nature methods* **9**, 357-359 (2012). https://doi.org:10.1038/nmeth.1923

101 Ramirez-Gonzalez, R. H., Bonnal, R., Caccamo, M. & Maclean, D. Bio-samtools: Ruby bindings for SAMtools, a library for accessing BAM files containing high-throughput sequence alignments. *Source code for biology and medicine* **7**, 6 (2012). https://doi.org:10.1186/1751-0473-7-6

102 Liao, Y., Smyth, G. K. & Shi, W. featureCounts: an efficient general purpose program for assigning sequence reads to genomic features. *Bioinformatics (Oxford, England)* **30**, 923-930 (2014). https://doi.org:10.1093/bioinformatics/btt656

103 Team, R. C. R: A language and environment for statistical computing. *http://www.r-project.org/* (2012).

104 Anders, S. & Huber, W. Differential expression analysis for sequence count data. *Genome Biology* **11**, R106 (2010). https://doi.org:10.1186/gb-2010-11-10-r106

105 Tyanova, S., Temu, T. & Cox, J. The MaxQuant computational platform for mass spectrometry-based shotgun proteomics. *Nat Protoc* **11**, 2301-2319 (2016). https://doi.org:10.1038/nprot.2016.136

106 Cox, J. *et al.* Accurate proteome-wide label-free quantification by delayed normalization and maximal peptide ratio extraction, termed MaxLFQ. *Mol Cell Proteomics* **13**, 2513-2526 (2014). https://doi.org:10.1074/mcp.M113.031591

107 Vazquez-Laslop, N., Thum, C. & Mankin, A. S. Molecular mechanism of drug-dependent ribosome stalling. *Mol Cell* **30**, 190-202 (2008). https://doi.org:10.1016/j.molcel.2008.02.026

108 Keseler, I. M. *et al.* The EcoCyc database: reflecting new knowledge about Escherichia coli K-12. *Nucleic Acids Research* **45**, D543-D550 (2016). https://doi.org:10.1093/nar/gkw1003

FIGURE LEGENDS

Fig. 1: Loss of EttA impacts the TCA and glyoxylate shunt pathways and stress genes. **a**, Growth curves of the WT, Δ*ettA* and C_{ettA} strains in MMAA medium without or with NaCl (0.2 and 0.4 M). Error bars represent mean ± standard deviation (s.d.) for triplicate experiments. Above and below the curves, heatmaps showing the absorbance (OD_{600}) of cultures at various phases of the growth of the WT strain (t_0 to t_4). The dotted lines indicate the OD values assigned to the heatmap. Right: Table representing the difference in lag phase of Δ*ettA* versus WT and C_{ettA} strains and their respective doubling times in the same media calculated as described in the methods. **b**, Graph showing the fluorescence intensity at OD_{600}=1.4 of the MG1655 *ettA:yfp* strain expressing *ettA* in a translational fusion with a *yfp* gene, in the MMAA medium at different NaCl concentrations (0, 0.2, 0.3, 0.4 or 0.5 M). Background fluorescence of a culture without YFP has been subtracted, the error bars represent mean ± s.d. for triplicate experiments. **c**, Representation of TCA cycle and the glyoxylate shunt pathways showing intermediary products (in boxes), genes coding the enzymes (next to the reaction arrows) and cofactors (in grey). Genes in red were identified in the proteomic study as less expressed in the Δ*ettA* strain (**Extended Data Fig. 1d**). Grey heatmaps show the absorbance (OD_{600}) of cultures of WT, Δ*ettA* and C_{ettA} strains, at the same growth stage as panel (**a**), for cultures on different carbon sources at a concentration of 0.3 M (malate, fumarate and succinate) or 0.15 M (glyoxylate). Heatmaps in green show the YFP total fluorescence level of the same three strains with a *yfp* translational fusion inserted in the genome in frame with the *aceB*, *aceA, fumC*, *yjbJ* and *hchA* genes (*aceB:yfp*, *aceA:yfp, fumC:yfp, yjbJ:yfp* and *hchA:yfp*) grown in MMAA medium or LB medium for *fumC:yfp*. Scales are presented on the top of each heatmap. Full growth curves and time points used for the heatmap are presented in the **Extended Data Fig. 1i**.

Fig. 2: EttA assists ribosomes during the synthesis of peptides with repeated acidic residues. a, The beginning of the coding sequences of the *aceB* (malate synthase), *aceA* (isocitrate lyase), *fumC* (fumarase C), *yjbJ* (putative stress response protein), *hchA* (protein/nucleic acid deglycase 1), *frdD* (fumarate reductase subunit D), *elaB* (tail-anchored inner membrane protein) and *rraB* (ribonuclease E inhibitor protein B) genes were cloned in a low-copy plasmid (pMMB) under the control of an IPTG inducible promoter and translationally fused to a *yfp* gene. The corresponding aa sequence is presented on the left side. Point mutations tested (dark green) of the acidic residues (purple) responsible for the EttA-dependent expression are indicated in the sequence, other mutations upstream of the acidic residues were also tested for *aceB* and *yjbJ*. Two *aceA:yfp* fusions were made, one with only the intergenic *aceB-A* sequence and the second one with the operon sequence (*aceB* gene and the intergenic region). Cultures were performed in LB_Amp100 medium in the presence of 1 mM IPTG, to avoid differential growth between the strains. Histograms show the ratios of YFP intensity in the Δ*ettA vs.* WT strain for the different constructs (details of the calculation of the ratio and propagation of the error is given in the methods section) for the different constructs. Ratios are measured at the end of growth. The growth curves, results for the complemented strain (C_{ettA}) and details of the constructions are presented in **Extended Data Fig. 3**. **b,** Histograms showing the ratios of YFP intensity in the presence or absence of 5 μM His_6-EttA after 150 min of *in vitro* translation (NEB PURExpress) of the different transcripts ($aceB_{1\text{-}10aa}$*:yfp*, $yjbJ_{1\text{-}5aa}$*:yfp* and $rraB_{1\text{-}10aa}$*:yfp*) and for the same ones harboring the mutations that abolish EttA-dependency *in vivo*. The *p* values were determined by unpaired two-tailed *t*-tests. **a and b,** Error bars represent mean ± s.d. for triplicate experiments. **c,** Toeprinting assay using $aceB_{1\text{-}10aa}$

and *aceB*-NQ mRNA with or without His_6-EttA or His_6-EttA-EQ_2 at 5 μM. The position of ribosomes stalling at the initiation codon was verified by the addition of Thiostrepton and Retapamulin. **d,** Toeprinting assay of $yjbJ_{1\text{-}5aa}$ and *yjbJ*-NQ mRNA with or without His_6-EttA or His_6-EttA-EQ_2 at 5 μM. **c and d,** The structure of the mRNA used for toeprinting is indicated above the gels. Empty and plain arrows indicate ribosomes blocked at the initiation or arrested on a specific motif during elongation, respectively.

Fig. 3: EttA-dependent synthesis of some proteins of the TCA/glyoxylate shunt pathways can explain the observed phenotypes of the Δ*ettA* strain. **a,** Representation of the TCA cycle, the glyoxylate shunt and the tartronate semialdehyde pathway showing intermediary products and genes encoding the enzymes. The expression of genes shown in red is dependent on EttA. Heatmaps show the OD_{600} at various times of growth as in **Fig. 1a** from cultures in MM.Glyoxylate (left) or MMAA 0.4 M NaCl (right) media. The control experiments for the WT, Δ*ettA*, and C_{ettA} are presented on the top. The other heatmaps are for the same strains with a deletion of either *aceB, aceA, glcB, gcl, fumC, frdD* or *icd* gene (deletions are represented on the pathway map by red crosses) or for the same strains overexpressing *aceB* or *aceB*-NQ from a plasmid (↗*aceB* and ↗*aceB*-NQ, represented by green arrows). For *aceA* overexpression (↗*aceA*) from a plasmid, the three strains deleted of *aceA* were used. The OD equivalents of the heatmap color shadings are indicated above the control experiments (WT, Δ*ettA* and C_{ettA}) for the two tested media. Growth curves and time points used for the heatmaps are presented in **Extended Data Fig. 5**. **b and c,** Representation of the possible metabolic flux in MM.Glyoxylate medium (**b**) and MMAA 0.4 M NaCl medium (**c**) for the WT (blue) and Δ*ettA* (red) strains.

Fig. 4: Synthesis of the leader peptide MgtL by the ribosome is dependent on EttA. **a**, Model of the regulation of *mgtA* expression by Mg^{2+}. At high intracellular Mg^{2+} concentrations, the translation of the entire leader peptide MgtL, maintains the mRNA in a conformation where a Rho-dependent terminator (RDT) site is accessible for Rho to terminate the transcription of the mRNA. At low Mg^{2+} intracellular concentrations, dissociation of the elongating ribosome when polymerizing negatively charged residues of MgtL, changes the mRNA into a conformation where the RDT is no longer accessible, allowing the transcription of *mgtA*. **b,** Histograms showing the ratios of YFP fluorescence of Δ*ettA*/WT strains, for *mgtL*:*yfp* fusion (left), or *mgtL_mgtA*$_{1\text{-}5aa}$:*yfp* fusion (right). Constructs express either the WT *mgtL* or a mutant (*mgtL*-QN) where two acidic residues (purple) were mutated (dark green). The constructions used are shown above the histograms and the sequence of MgtL is on the left. The YFP sequence used in this experiment contains a 6-residues N-terminal translation enhancer[33]. The constructions were expressed from a pMMB plasmid and bacteria were grown in MMAA medium in the presence of Amp100, 1 mM IPTG and 2 mM $MgSO_4$. Ratios are measured at the end of growth (see **Extended Data Fig. 6b**). **c,** Design of the mRNA used for IVTA. Histograms showing the ratios of YFP intensity with or without His_6-EttA (5 μM) after 150 min of *in vitro* translation of mRNA coding for WT or MgtL-QN YFP fusions. **b and c,** Error bars represent mean ± s.d. for triplicate experiments. Two-tailed *t*-tests was used to measure the *p* value. **d,** Toeprinting assay of *mgtL* and *mgtL*-NQ mRNA with or without His_6-EttA or His_6-EttA-EQ_2 at 5 μM. Empty and plain arrows indicate ribosomes blocked at the initiation or arrested on a specific motif during elongation, respectively.

Fig. 5: EttA rescues translation of mRNA encoding acidic residues at the beginning of translated sequences and shares a structural homology with EF-P. **a,** Histograms showing the

ratio of the YFP fluorescence emission of Δ*ettA/*WT strains expressing the 5'UTR of *yjbJ* followed by a *yfp* gene where the exogenous coding sequence NKDEPD has been inserted after the initiating methionine using two different sets of synonymous codons (syn-codon, see methods). A similar construct with the 5'UTR of a*ceB* is also presented as well as equivalent constructs where segments (10, 20, 30 or 40 aa) of the AceB-NQ sequence have been introduced between the initiating methionine and the NKDEPD sequence. Cartoons of the translated peptides in the exit tunnel of the ribosome are shown on the right. Results for the complemented strain (C_{ettA}) and the growth curves are presented in **Extended data Fig. 7a, b**. **b,** Histograms showing the ratio of YFP intensity after 150 min of *in vitro* translation of a UTR_{aceB}_MNKDEPD:*yfp* mRNA with or without His_6-EttA (5 μM). Error bars represent the mean ± s. d. for triplicate experiments. **c,** Violin plot showing the expression level of genes containing the ExD motif (- /$X_{0,1}$/ -) or not within the first 50 neo-synthesized aa by windows of 10 aa based on the log_2 Δ*ettA*/WT ratios obtained in the S_{15} proteomic. The red and grey dotted lines represent the median and quartiles respectively. The *p* values are calculated using the Mann-Whitney test. The same analysis for the complemented strain (C_{ettA}) is presented in **Extended data Fig. 7d**. **d,** Model of EttA function to rescue the expression of genes with the DxE motif. When ribosomes encounter repeats of acidic residues (adjacent or separated by one residue) during the early stage of the synthesis of the nascent elongating peptide, they stall and in certain cases, they dissociate from the mRNA (as for *aceB* and *mgtL* genes). EttA can probe stalled ribosomes with an empty E site and restore the elongation process, then it dissociates using its ATPase activity. **e,** Structure of EttA-EQ_2 (dark blue) in complex with 70S IC complex (EMD-29398)[23] aligned on the domain V of the 23S rRNA of the structure (6ENJ)[71] of the polyproline-stalled ribosome in complex with EF-P (green).

METHODS

Bacterial strains

The strains used in this study are listed in **Supplementary Tables 1 to 3**. The WT reference strain used was the sequenced MG1655[93] strain. The Δ*ettA* strain from a previous study[6] was complemented by insertion of the *ettA* gene with is native promoter at the P21 genomic locus (strain C_{ettA}) or at the *attB* locus (strain C'_{ettA}, this strain was used for the Δ*icd* constructions because the P21 locus was not compatible with this deletion). The insertion comprises the ORF of EttA with 105 base pairs upstream and downstream. Insertions in the genome were conducted using the pOSIP clonetegration recombination method [94]. Primers used for the amplification and control of the insertion are described in **Supplementary Table 5**. Strains harboring a *yfp* fusion with the *aceA, aceB, fumA, fumB, fumC, frdA, frdB, frdD, mqo and glcB* genes were constructed by P1 transduction using a collection of YFP fusions created by the Mori laboratory[95] as donor strains and the three receiver strains MG1655 (WT), *ΔettA* and C_{ettA}. Strains harboring a *yfp* fusion with the *yjbJ*, *hchA* and *elaB* genes were constructed by amplifying the *yfp* and chloramphenicol resistance cassettes from the Mori collection[95] with primers containing in their 5' extremities 60 base pairs homologous to the upstream and downstream regions of the stop codon of the target gene (**Supplementary Table 5**). Then, the PCR products were introduced by electroporation into MG1655 cells harboring the pKD46 plasmid expressing the λ_{red} recombinase and the Gam proteins[96] followed by a selection of chloramphenicol-resistant fusion clones. The constructs were finally transduced with P1 phage into the receiver strains (WT, Δ*ettA* and C_{ettA}). For the strains

individually deleted of *ettA* target genes, deletions from donor strains of the Keio collection[97] were transferred by P1 transduction into the receiver strains (WT, Δ*ettA*, C_{ettA} and C'_{ettA}). All the constructed strains were verified by PCR using the primers described in **Supplementary Table 5**.

Plasmids construction

All the plasmids constructed in this study are listed in the **Supplementary Table 4** and were cloned in the DH5α strain. The pMMB plasmids used for target validation in the WT, Δ*ettA*, and C_{ettA} strains, were derived from the low-copy plasmid pMMBpLlacO-1-67EH. It allows controlled gene expression from the IPTG inducible PLlacO-1 promoter[33] with a transcription start that permits to retain the native 5'UTR of the inserted gene. All of EttA target genes, (except the *mgtL_mgtA*$_{1\text{-}5aa}$ insert sequence, which was synthesized by the company TWIST bioscience) were PCR amplified from genomic DNA of the MG1655 strain with primers hybridizing at the transcription initiation site and to the stop codon of the ORF. In the case of multiple transcription start sites we selected the one that generates the shortest 5'UTR. The primers and the synthetic insert have in their extremities a homology (15 to 20 bases) to the PCR products of the pMMB produced for the cloning (**Supplementary Table 6**). The plasmids were assembled using the NEBuilder HiFi DNA Assembly kit (New England BioLabs). The different truncated or point mutants derived from these plasmids were generated by PCR amplification using primers (**Supplementary Table 6**) that hybridize at the truncation or contain the point mutations(s) and with 15 bases of homology to allow plasmid recircularization using the NEBuilder HiFi DNA Assembly kit. The pMMB-*aceB* and pMMB-*aceA* plasmids without the YFP fusion were also generated by the same strategy. Plasmid constructs carrying the nucleotide sequence encoding the NKDEPD motif were generated from the plasmid pMMB-*aceB*-NQ:*yfp* by the same approach. The synonymous coding sequence for pMMB-UTR$_{yjbJ}$_MNKDEPD$_{\text{syn-codon}}$:*yfp* changes the original sequence ATGAATAAAGATGAACCAGAT to ATGAATAAAGA<u>C</u>GA<u>G</u>CCAGA<u>C</u> where the three codons encoding acidic residues were replaced by synonymous codons (codons encoding the same residues). All the constructed plasmids were confirmed by sequencing. Most of the constructions with a *yfp* gene express the native YFP venus except for the *mgtL mgtA* constructions which express an optimized YFP[33] and for the *yfp* mutant presented in **Extended Data Fig. 7a** where the first 6 codons systematically use the synonymous codon with the highest number of adenosine.

Growth media and culture conditions

Overnight cultures of the various MG1655 strains were carried out in Luria-Bertani Miller broth (LB-Difco) at 37 ºC with agitation. For strains transformed with pMMB or pBAD plasmids, growth medium was supplemented with ampicillin at 100 µg.ml^{-1} (LB_Amp100) or kanamycin at 50 µg.ml^{-1} (LB_Kan50) and, when required, 0.4% (w/v) of ß-D-glucose was added to repress expression of pBAD plasmids (pBAD-*His$_6$-ettA*-EQ$_2$). Bacteria were cultivated in the different media indicated in the figures. A modified MJ9 medium[98], composed of KH_2PO_4 at 16.5 mM, K_2HPO_4 at 8.5 mM, NH_4SO_4 at 15 mM, $MgSO_4$ at 2 mM, MOPS at 133 mM, Tricine at 13.3 mM, supplemented by a 100X dilution of a vitamins mix (MEM VITAMINS, Sigma-Aldrich) and trace elements as described in the original MJ9 medium[98], was used for the cultures. For the MMAA, all the amino acids (Sigma-Aldrich) with the exception of cysteine, tyrosine, tryptophan and methionine (due to their low solubility) were added at 2 mg.ml^{-1} as carbon source for a final concentration of: glycine at 26.6 mM, alanine at 22.4 mM, valine at 17 mM, leucine at 15.2 mM, isoleucine at 15.2 mM, proline at 17.3 mM, phenylalanine at 12.1 mM, serine at 19 mM, threonine at 16.8 mM, asparagine at 15.1 mM, glutamine 13.7 mM, aspartic acid at 15 mM, glutamic acid at 13.6 mM, arginine at 11.4 mM, histidine at 12.8 mM and lysine at 13.6 mM. Other carbon sources tested were: L-malic acid, sodium fumarate dibasic, succinic acid and pyruvic acid and α-

ketoglutaric acid at 0.3 M, glyoxylic acid (MM.Glyoxylate) and oxaloacetic acid at 0.15 M and glucose at 22 mM (MMGlc) all in the MM medium (carbon sources are purchased from Sigma-Aldrich with the exception of α-ketoglutaric acid purchased from Bio Basic). For the assay with salt, NaCl was added at the indicated final concentrations in the figures. Expression of the inserted genes or YFP fusions was induced by addition to the medium of 1mM of Isopropyl β-D-1-thiogalactopyranoside (IPTG) for the pMMB constructions or 0.2% (w/v) of L-Arabinose for the pBAD constructions.
Cultures in 96-well Falcon microplates were done in triplicate in a volume of 200 µl of medium inoculated with 2 µl of over-night culture (for the MMAA NaCl test, the cultures were washed with a solution of 0.9% (w/v) NaCl prior to inoculation) and a volume of 60 µl of mineral oil (Sigma Aldrich) was added to each well in order to prevent evaporation of the medium during growth. Growth of the different strains was followed by measuring the optical density at 600 nm (OD_{600}) when incubated at 37 ºC under 600 rpm double-orbital shaking with a CLARIOstar plate reader (BMG Labtech). The emission of the YFP fluorescence was recorded at 540-20 nm with an excitation at 497-15 nm. Measurements were taken every 30 min.

Fitness assays
Competitive fitness assays were conducted as described previously[6] except that different media, described in the **Extended Data Fig. 1a**, were tested (Luria-Bertani (LB) medium from two different providers: Difco Becton Dickinson and USB-affymetrix, MMAA and MMGlc media described above). Briefly, from overnight cultures in LB-Difco medium of the WT and Δ*ettA* strains, an inoculum composed of an equal ratio of the two strains was used to start a co-culture in the media indicated in the **Extended Data Fig. 1a**. Growth was carried out at 37 ºC with shaking for a determined period, then the cultures were sub-cultured in fresh medium (+ 24 h) to test the viability of the strains during the experiment. PCR assays were performed on cells at the end of each co-culture, using primers hybridizing at ~500 bp upstream and downstream of the *ettA* gene as previously described[6].

Motility assay
Stationary-phase bacterial cultures were used for the motility test. Overnight precultures of the three strains (WT, Δ*ettA* and C_{ettA}) were washed and diluted to an OD_{600}= 0.5 in physiological water to prepare the inoculum. The motility test was then carried out on a plate containing the MMAA culture medium supplemented with 0.3% (w/v) agar. Plates were inoculated by picking them using a toothpick soaked in an inoculum and then incubated at 37°C. Representative images of the swimming motility are shown after 48 h.

Protein extracts and total RNA preparation
Samples for quantification by western and northern blots of protein and mRNA of the *yfp* genomic fusion with *aceA, aceB, fumC, yjbJ and hchA* genes were prepared as following. 96-well microplate culture of each strain (WT, Δ*ettA* and C_{ettA}) with the *yfp* fusion were grown in MMAA or LB medium as described above. For the western blotting, 100 µl of the culture was pelleted, then resuspended in Laemmli (Bio-Rad), in a volume to normalize the OD_{600}. For northern blotting, 400 ul of culture were resuspended in 100 µl of RNAsnap buffer (95% (v/v) formamide, 18 mM EDTA, 0.025% (v/v) SDS, 1% (v/v) β-mercaptoethanol) using the RNAsnap method as described previously[99].

Western Blotting
After separation on a 12.5% acrylamide SDS-PAGE gel, proteins were transferred onto a polyvinylidene difluoride (PVDF) membrane for 30 min at 2.5 V and 25 mA using a semi-dry

Trans-Blot Turbo system (Bio-Rad). Membranes were blocked by incubating them for two hours at room temperature in a PBS buffer supplemented with 5% (w/v) of skimmed milk powder and then incubated for 2 h at room temperature or overnight at 4 ºC in 3 ml of PBS 1X + 0.1% (v/v) Tween-20 in presence of a 1,000x dilution of anti GFP antibody (Rabbit anti-GFP, Invitrogen Thermo Fisher Scientific). After washing, the bound antibody was detected after incubation for 1 h in the presence of a secondary antibody in PBS buffer: for *aceB, aceA* and *yjbJ yfp* fusions, a near infrared fluorescent probe (IRDye 680LT anti-rabbit LI-COR Biosciences) diluted 20,000x in PBS was used whereas for *hchA* and *fumC yfp* fusions, an HRP-conjugated antibody (Anti-rabbit IgG, antibody [HRP] from COVALAB) diluted 20,000x in PBS was used. The HRP-conjugated antibody was detected with the Clarity Western ECL Substrate (Bio-Rad) and signal detection was performed on a Licor Odyssey scanner.

Northern Blotting

For each condition, 6 µg of total RNAs were loaded on a 1% (w/v) agarose gel. Electrophoretic migration was carried out for 75 min at 100 V. RNAs were then transferred to an Amersham Hybond-N+ membrane (Cytiva). Transfer of the RNAs was verified by UV. The RNAs were cross-linked on the membrane by exposing the membrane to UV for 30 s at 100 x 1 200 µJ / cm^2. The radioactive probe was prepared from 40 pmoles of primers described in **Supplementary Table 7** and labeled at the 5' end with 10 units of T4 polynucleotide kinase (New England Biolabs) and [γ-^{32}P]-ATP (150 µCi). Membranes were incubated with the probe in the hybridization buffer (ULTRAhyb, Invitrogen Thermo Fisher Scientific) overnight at 42 ºC. Membranes were washed three times (once in 2x SSC + 0.1% (v/v) SDS, once in 1x SSC + 0.1% (v/v) SDS and finally in 0.1x SSC + 0.1% (v/v) SDS) at 42 ºC during 15 min. Radioactive signal was detected on a Typhoon 9 500 FLA scanner (GE Healthcare).

RNA-seq and proteomic experiments

Cultures of the three strains (WT, Δ*ettA* and C_{ettA}) in a volume of 125 ml of MMAA 0.4 M NaCl medium were inoculated at 1/20 with overnight cultures prepared in LB-Difco medium. Cells were grown at 37 ºC with shaking. After 330 min of culture, 3 ml samples were collected for each strain for the transcriptomic analysis. Cultures were stopped by addition of two volumes of RNAprotect (Qiagen) then centrifuged at 5,000 g for 5 min. Pellets were isolated and immediately stored at -80 °C. Total RNA were extracted with the Direct-zol RNA MiniPrep kit (ZYMO RESEARCH). Ribosomal RNAs were specifically eliminated using the Ribo-Zero rRNA Removal kit (Illumina). The library and deep sequencing were performed by the GATC company on an Illumina HiSeq sequencer. Sequences were aligned with Bowtie2[100], indexed with Samtools[101] and counted with FeatureCount[102]. Normalization and statistical analysis were performed with R software[103] and Deseq script[104].

For the proteomic experiments, 100 ml samples were taken from triplicated cultures. Cells were washed in PBS and pelleted by centrifugation at 5,000 xg for 10 min at 4 °C. Pellets were resuspended in 150 µl of lysis buffer (PBS 1X, 1% protease inhibitor cocktail EDTA-free, Roche-100X in DMSO and lysed by sonication (amplitude 70%, 3 pulses of 15 sec separated by 15 sec intervals). Two proteomics analyses were performed, named "proteomic S_{15}" and "proteomic P_{150}" respectively. First, for the proteomic S_{15}, lysates were centrifuged at 15,000 g for 30 min at 4 ºC and protein extracts were recovered and divided into 3 aliquots of 50 µl. The concentrations of the protein extracts were determined using a BCA assay (Pierce BCA Protein Assay, Thermo Fisher Scientific) and a verification of the protein extracts was carried out on a 12.5% acrylamide SDS-PAGE gel stained with Coomassie brilliant blue R-250. 25 µg of each protein sample were diluted

in a final volume of 25 µl for a final concentration of 8 M Urea / 50 mM Ammonium Bicarbonate. Cysteine reduction and alkylation were achieved by the addition of DL-Dithiothreitol and iodoacetamide respectively. The protein extracts were digested by Lys-C endoproteinase and then by trypsin (Trypsin Gold, Promega). Peptides were vacuum-dried and resuspended in 100 µl of solvent A (0.1% (v/v) formic acid in 3% (v/v) acetonitrile) to get a final concentration of 250 ng.µl^{-1} before analysis by MS / MS mass spectrometry. For the proteomic P_{150}, lysates were centrifuged at 150,000 g for 1 hour at 4 °C. Pellets were resuspended in 200 µl of 1X PBS with 0.3% (v/v) SDS and the concentrations of the protein extracts were determined using a BCA assay. 25 µg of each sample were loaded on a 12.5% acrylamide SDS-PAGE gel and after a short (1 cm) migration, proteins were stained with Coomassie brilliant blue R-250. Lanes containing proteins were excised and subjected to digestion with porcine trypsin. Protein extracts were then processed in the same way as protein extracts from proteomic S_{15}.

Mass spectrometry analyses were performed on a Q-Exactive Plus hybrid quadripole-orbitrap mass spectrometer (Thermo Fisher, San José, CA, USA) coupled to an Easy 1,000 reverse phase nano-flow LC system (Proxeon) using the Easy nano-electrospray ion source (Thermo Fisher). Briefly, peptide mixtures were analyzed in triplicate. 4 µl of peptide mixtures were loaded onto an Acclaim PepMap precolumn (75 µm x 2 cm, 3 µm, 100 Å; Thermo Scientific) equilibrated in solvent A and separated at a constant flow rate of 250 nl/min on a PepMap RSLC C18 Easy-Spray column (75 µm x 50 cm, 2 µm, 100 Å; Thermo Scientific) with a 90 min gradient (0 to 20% solvent B (0.1% (v/v) formic acid in acetonitrile) in 70 min and 20 to 37% solvent B in 20 min). Data acquisition was performed in positive and data-dependent modes. Full scan MS spectra (mass range m/z 400-1800) were acquired in profile mode with a resolution of 70,000 (at m/z 200) and MS/MS spectra were acquired in centroid mode at a resolution of 17,500 (at m/z 200).

Data processing for label-free quantification - Raw data were processed with the MaxQuant software package (http://www.maxquant.org, version 1.5.6.5)[105]. Protein identifications and target decoy searches were performed using the Andromeda search engine and the SwissProt database restricted to the *E. coli* K-12 taxonomy (release: 15/11/2018; 4477 entries) in combination with the Maxquant contaminants database (number of contaminants: 245). The mass tolerance in MS and MS/MS was set to 10 ppm and 20 mDa, respectively. Methionine oxidation and protein N-term acetylation were taken into consideration as variable modifications whereas cysteine carbamidomethylation was considered as fixed modification. Trypsin was selected as cutting enzyme and 2 missed cleavages were allowed. Proteins were validated if at least 2 unique peptides having a protein FDR < 0.01 were identified. The setting "Match between runs" was also taken into consideration to increase the number of identified peptides. For quantification, we used unique and razor peptides with a minimum ratio count ≥ 2 unique peptides. Protein intensities were calculated by Delayed Normalization and Maximal Peptide Ratio Extraction[106] (MaxLFQ). Statistical analysis was done using Perseus software (https://maxquant.org/perseus, version 1.6.0.7) on LFQ intensities. Proteins belonging to contaminants and decoy databases were filtered. For each biological replicate, the median intensity of the two injected replicates was determined and proteins having quantitative data for all the biological replicates were considered for statistical analysis using a Benjamini-Hochberg test. Principal component analysis of the S_{15} proteomic result showed an outlier sample for one of the Δ*ettA* biological triplicate, therefore, it was excluded and the analysis was carried on biological duplicate for the three strains.

Protein expression and purification

EttA and EttA-EQ_2 proteins were expressed with an N-terminal hexahistidine-tag (His_6) from the pBAD plasmid under the control of an arabinose-inducible promoter in the strain MG1655. Protein production and purification was conducted following the previously published method[6] with the following changes. Cell lysis was performed by 3 successive passages in a cell disrupter (Constant Systems Ltd) at 2.5 kbar pressure. Initial purification step was realized on a Protino Ni-NTA column (Macherey-Nagel) then on a butyl-Sepharose FF (Cytiva) and finally monodispersed purified protein were separated on a HiPrep 16/60 Sephacryl S-200 column (Cytiva). Purification buffers were the same as in Boël *et al*.[6]. The concentration of the protein was estimated using the BCA kit (Pierce BCA Protein Assay Kit - Thermo Fisher Scientific) according to the supplier's recommendations as well as by comparing the protein on a 12.5% acrylamide Coomassie-stained SDS-PAGE gel with BSA standards. The pure protein was frozen in liquid nitrogen and stored at -80 ºC.

Purification of *E. coli* MRE600 ribosomes

Highly purified ribosomes of *E. coli* MRE600 strain, devoid of EttA protein (undetectable by Western blotting), were prepared by multiple centrifugations over sucrose cushions and gradients. Briefly, two liters of LB medium were inoculated with 20 ml of a saturated overnight culture of *E. coli* MRE600, grown at 37°C under agitation to an OD_{600} of 0.5. Cells were immediately harvested by centrifugation for 20 min, at 5,000 g at 4 °C then resuspended and washed in buffer A (20 mM Tris pH 7.4, 10 mM Mg(OAc), 100 mM NH_4(OAc), 0.5 mM EDTA). All subsequent steps were performed at 4°C. Cells were resuspended in buffer A supplemented with 0.1 $mg.ml^{-1}$ lysozyme, 6 mM β-mercaptoethanol and 0.1% (v/v) protease inhibitor cocktail (Sigma Aldrich) and lysed by 3 passages at 2.5 kBar using a cell disrupter (Constant Systems Ltd). Clarification of the lysate was then performed by two centrifugations of the extract at 22,000 g for 20 min at 4°C. The supernatants were recovered and overlaid on an equal volume of 37.7 % (w/v) sucrose cushion in buffer B (20 mM Tris pH 7.4, 10 mM Mg(OAc), 500 mM NH_4(OAc), 0.5 mM EDTA, 6 mM β-mercaptoethanol) and the samples were then centrifuged for 20 h, at 206,000 g at 4°C in a Type 70 Ti rotor (Beckmann Coulter). Sucrose cushions were decanted and the clear ribosomal pellet was resuspended and incubated in buffer C (20 mM Tris pH 7.4, 7.5 mM Mg(OAc), 60 mM NH_4(OAc), 0.5 mM EDTA, 6 mM β-mercaptoethanol) under gentle agitation for 3 h, at 4°C. Then 12 mg of crude ribosomes were loaded onto 10-40% (w/v) sucrose gradients prepared with buffer C and centrifuged for 16 h at 71,935 g at 4 °C in a SW28 rotor (Beckman Coulter). Gradients were fractionated on a Biocomp Piston Gradient Fractionator (BioComp Instruments) and absorbance was measured at 254 nm. Fractions corresponding to the 70S ribosomes were pooled, washed and concentrated in Amicon 50k (Merckmillipore) using Buffer C. The purified ribosomes were quantified by NanoDrop OneC UV-Vis Spectrophotometer (Thermo Scientific) checked on agarose gel, aliquoted, flash frozen in liquid nitrogen and stored at -80 °C.

In vitro transcription

The DNA templates used to generate mRNAs for *in vitro* translation assays and Toeprinting assays, were PCR amplified with primers (**Supplementary Table 7**) from the pMMB plasmids containing the desired genes to be transcribed. The forward primer contains the T7 polymerase promoter sequence (5'-GCGAATTAATACGACTCACTATAGGG-3'). *In vitro* mRNA synthesis was then carried out at 37 ºC for 4 h in T7 RiboMAX Large Scale RNA Production System kit (Promega) according to the manufacturer's recommendations. At the end of the reaction, DNA templates were degraded by adding DNAse I for 15 min and the mRNA transcripts were purified using TRIzol Reagent (Thermo Fisher Scientific) and Direct-zol RNA Miniprep kit (Zymo

Research). The mRNAs were finally eluted in The RNA Storage Solution (Ambion,Thermo Fisher Scientific) and stored at -80 ºC.

In vitro translation assays

The PURExpress ΔRibosome In Vitro Protein Synthesis Kit (New England Biolabs) was used for *in vitro* translation assays. Reactions were performed in a final volume of 10 µl according to the instructions given by the manufacturer. This system consists of two solutions A and B in which all elements of the translational machinery are present except the ribosomes. Ribosomes purified from *E. coli* strain MRE600 were used at a final concentration of 2 µM per reaction. In a 10 µl translation reaction, the mRNA encoding each target gene fused with the *yfp* fluorescent reporter gene, was used at a final concentration of 1 µM. The His_6-EttA protein previously diluted to 40 µM in the purification buffer and heated at 37 ºC for 4 h (to increase the monomeric conformation) was added to the translation reactions at 5 µM final. As negative control the purified protein was replaced by the purification buffer. Reactions were transferred to a 384-well plate (Sigma Aldrich), incubated for 150 min in the CLARIOstar plate reader (BMG Labtech) and translation of the mRNA was monitored every 2 min by measuring YFP fluorescence as previously described. All the translation assays were performed in triplicate for each condition.

Toeprinting assays

Assays were performed using the PURExpress ΔRibosome (New England Biolabs) according to manufacturer instructions, to determine stalled-ribosome sequence motifs on the target mRNAs. Purified His_6-EttA or His_6-EttA-EQ_2 proteins were added to *in vitro* translation reactions at final concentrations of 2 µM and 5 µM respectively to evaluate the effect of the ABC-F on the stalled ribosomes. In the reactions in which the effect of antibiotics was tested, the antibiotics (thiostrepton or retapamulin) were added first so as to have a final concentration of 50 µM in the tubes and then dried using a SpeedVac vacuum concentrator (Thermo Fisher Scientific). Purified ribosomes from MRE600 were added to the reactions at a final concentration of 2 µM and mRNA templates at 1 µM. Reactions were then incubated at 37 ºC for 15 min and 2 pmoles of CY5-labeled primer (**Supplementary Table 7**) complementary to NV1 sequence[107] (5' GGTTATAATGAATTTTGCTTATT 3') were added and incubated immediately for 5 min at 37 °C. Finally, reverse transcription reactions were performed by adding 0.5 µl (corresponding to 5 U) of AMV Reverse Transcriptase (Promega), 0.1 µl dNTP mix (10 mM), 0. 4 µl Pure System Buffer (5 mM K-phosphate pH 7.3, 9 mM Mg(OAc), 95 mM K-glutamate, 5 mM NH_4Cl, 0.5 mM $CaCl_2$, 1 mM spermidine, 8 mM putrescine, 1 mM DTT) for each reaction and incubated at 37 ºC for 20 min. Once Cy5-labeled cDNA were generated, the mRNAs were degraded by addition of 0.5 µl of 10 M NaOH and incubation at 37 ºC for 20 min. All the reactions were neutralized by addition of 0.7 µl of 7.5 M HCl followed immediately by addition of 20 µl of toeprint resuspension buffer (300 mM Na-acetate pH 5.5, 5 mM EDTA, and 0.5% SDS (v/v)). Using QIAquick Nucleotide Removal kit (Qiagen), cDNAs were purified according to supplier instructions and then dried and resuspended in 6 µl of toeprint loading dye (95% formamide, 250 µM EDTA, and 0.25% (w/v) bromophenol blue). Sanger sequencing reactions were also performed on the DNA templates that were used for mRNA synthesis for the toeprint assays. Polymerization reactions were prepared in 20 µl with ddNTPs (625 µM ddCTP/ddTTP/ddATP or 50 µM ddGTP), 0.025 U Taq Pol (New England Biolabs), 1x Thermo Pol Buffer (New England Biolabs), 5 nM DNA matrix, 75 nM CY5-labeled primer 137 and 40 µM of each dNTP. After amplification by PCR, 20 µl formamide dye was added to each sequencing reaction and all of the samples were denatured at 80 ºC for 3 min before being loaded onto the acrylamide/bis-acrylamide/urea sequencing gel. Cy5-

labeled cDNAs were detected by fluorescent mode using a Typhoon FLA 9500 (GE Healthcare Life Sciences) Gel Scanner and LPR Ch.2 filter and 635 nm laser.

Analytical gel-filtration and static light-scattering analyses

Protein samples were injected onto a Yarra 3 µm SEC-2000 (Phenomenex) running at room temperature in 150 mM NaCl, 5% (v/v) glycerol, 20 mM Tris-HCl, pH 7.2. The column effluent was monitored with multi-angle light scattering detector (miniDAWN treos) and refractive index (Optilab T-rEX) detectors from Wyatt Technologies.

Image analyses and preparation

Western and northern blots signals were quantified using Fiji[89] software. Figures of the structure of EttA-EQ_2 in complex with 70S IC complex (EMD-29398)[23] and structure (6ENJ)[71] of the polyproline-stalled ribosome in complex with EF-P were prepared using PyMOL Molecular Graphics System (Schrödinger) and the structures were aligned on the domain V of the 23S rRNA.

Statistics and Reproducibility

All the experiments presented have been reproduced at least twice with the same results. The detail of the different statistical analysis presented herein are the following:

Bacteria growth rate -We extracted the early exponential phase of the growth curves, then the doubling time was calculated by fitting the curves to Malthusian growth equation;

$$Y = Y_o e^{(kt)}$$

$$\text{doubling time} = \frac{\ln(2)}{t}$$

Where Y is the population, Y_0 the starting population, k the rate and t the time. The lag was determined by measuring the delta between the tangent interception with the time axes of the WT strain and compared strain.

Determination of the fluorescence ratio - Calculation of fluorescence ratios were done by first calculating the ratio of the fluorescence to OD_{600} (Fluo/OD) of each triplicate to obtain the normalized fluorescence (FluoN), then the average for the WT, Δ*ettA* and C_{ettA} strains was corrected by subtracting the average of the FluoN for the WT pMMB-Ø strain (WT strain carrying an empty pMMB plasmid) ($FluoN_{control}$) to obtain the corrected normalized fluorescence (FluoNC). Finally, we calculated the ratios of the FluoNC for the Δ*ettA* and the C_{ettA} strains compared to the WT strain. The propagation of uncertainty was determined by the function:

$$f = A - B$$

Where A is the FluoN of the strain WT, Δ*ettA* or C_{ettA} and B the $FluoN_{control}$. The resulting standard deviation of the FluoNC was calculated using the equation:

$$\sigma_f = \sqrt{\sigma_A^2 + \sigma_B^2 - 2\sigma_{AB}}$$

Where σ_A and σ_B are the standard deviations of the variables A and B and σ_{AB} the covariance. Finally, the standard deviation of the ratio (σ_r) is:

$$\sigma_r = \frac{FluoNC_{WT}}{\sigma_f}$$

For the fluorescence reporters for *mgtL* or *mgtA* the normalization was done on the WT strain in the 2 mM Mg^{2+} culture condition.

Protein sequence motif analyses - Presence and position of the proteins containing the motif E/D X{0,1} E/D within the first 50 aa of the N-terminal part of the sequence were determined in the *E. coli* proteome using the Ecocyc database[108] and mapped to the proteomic quantification (S_{15}) data (with the EttA targets presented in this study previously excluded). Then the $\log_2$ ratios of the protein quantification ratios for Δ*ettA* vs WT and C_{ettA} vs WT were binned into six bins: absence of the motif (N=488 for Δ*ettA* vs WT and N=476 for C_{ettA} vs WT), motif between residues 1 to 10 (N=121 for Δ*ettA* vs WT and N=116 for C_{ettA} vs WT), motif between residues 11 to 20 (N=204 for Δ*ettA* vs WT and N=200 for C_{ettA} vs WT), motif between residues 21 to 30 (N=184 for Δ*ettA* vs WT and N=176 for C_{ettA} vs WT), motif between residues 31 to 40 (N=184 for Δ*ettA* vs WT and N=177 for C_{ettA} vs WT) and motif between residues 41 to 50 (N=152 for Δ*ettA* vs WT and N=150 for C_{ettA} vs WT). Violin plots were generated using Prism 8 (GraphPad) and *p* values were calculated using a two tailed Mann-Whitney test.

Figure 1

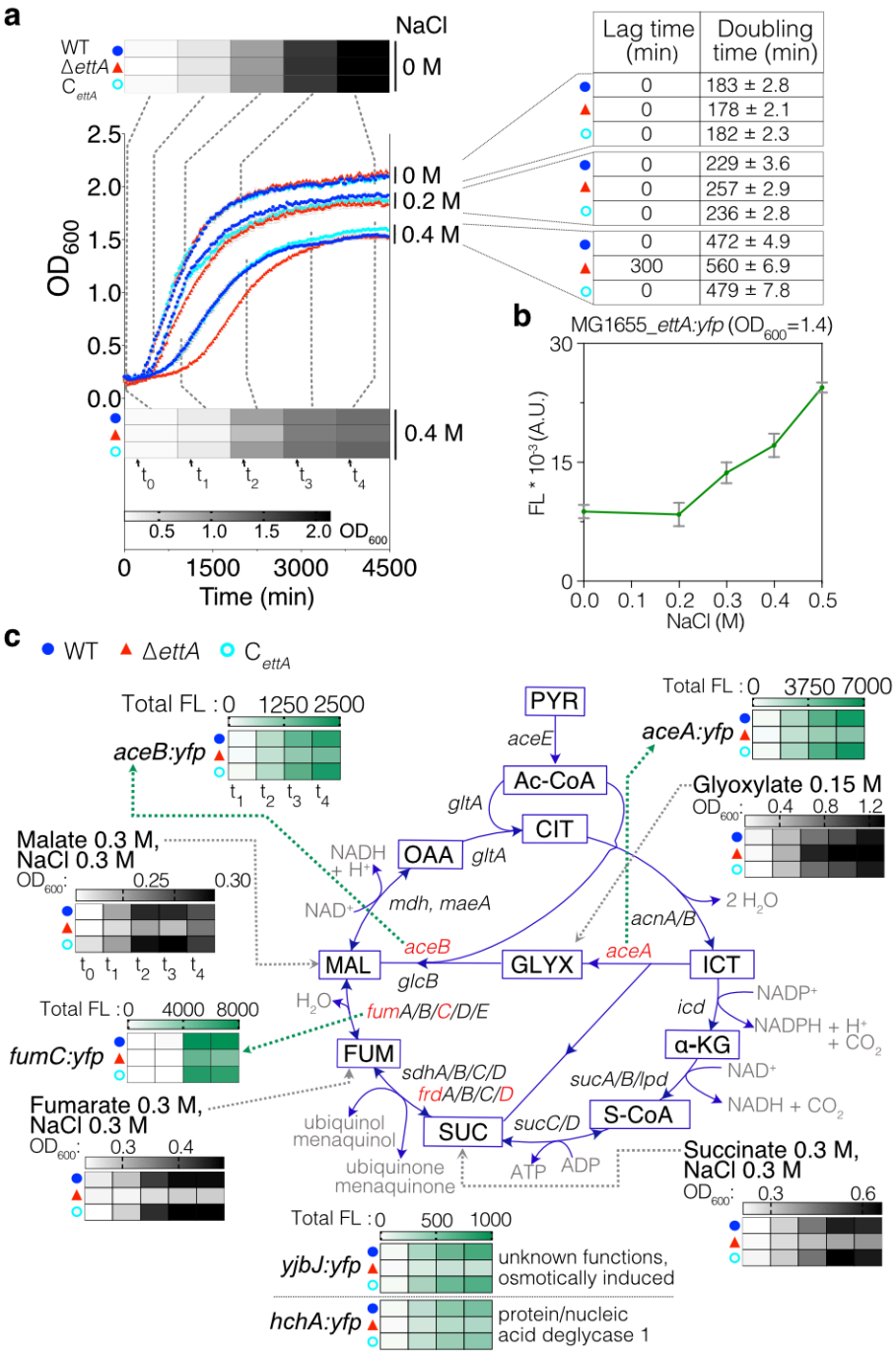
a
WT
ΔettA
C ettA
NaCl
0 M
0 M
0.2 M
0.4 M
0.4 M
OD600
Time (min)
0.5 1.0 1.5 2.0 OD600
Lag time (min)
Doubling time (min)
0 183 ± 2.8
0 178 ± 2.1
0 182 ± 2.3
0 229 ± 3.6
0 257 ± 2.9
0 236 ± 2.8
0 472 ± 4.9
300 560 ± 6.9
0 479 ± 7.8
b
MG1655_ettA:yfp (OD600=1.4)
FL * 10-3 (A.U.)
NaCl (M)
c
WT ΔettA C ettA
Total FL : 0 1250 2500
aceB:yfp
Total FL : 0 3750 7000
aceA:yfp
Glyoxylate 0.15 M
OD600: 0.4 0.8 1.2
Malate 0.3 M, NaCl 0.3 M
OD600: 0.25 0.30
Total FL : 0 4000 8000
fumC:yfp
Fumarate 0.3 M, NaCl 0.3 M
OD600: 0.3 0.4
Succinate 0.3 M, NaCl 0.3 M
OD600: 0.3 0.6
Total FL : 0 500 1000
yjbJ:yfp
unknown functions, osmotically induced
hchA:yfp
protein/nucleic acid deglycase 1
PYR
aceE
Ac-CoA
gltA
CIT
OAA
gltA
NADH + H+
NAD+
mdh, maeA
aceB
MAL
glcB
GLYX
aceA
ICT
acnA/B
2 H2O
H2O
fumA/B/C/D/E
FUM
sdhA/B/C/D
frdA/B/C/D
ubiquinol
menaquinol
ubiquinone
menaquinone
SUC
sucC/D
ATP ADP
S-CoA
sucA/B/lpd
NAD+
NADH + CO2
α-KG
icd
NADP+
NADPH + H+ + CO2

Figure 2

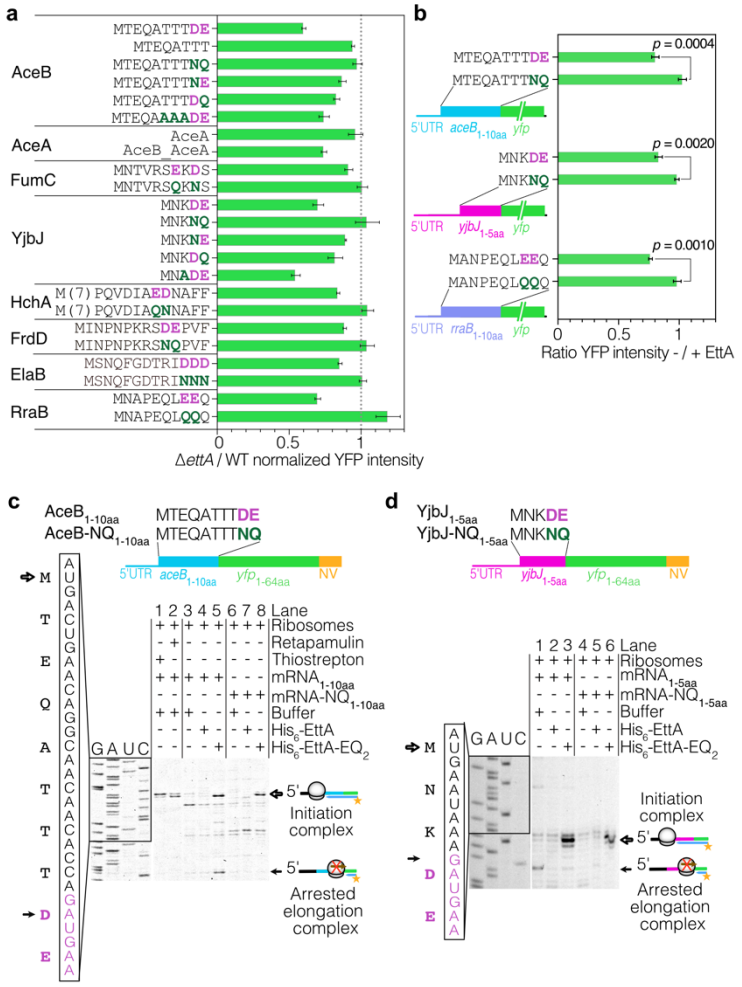
a
AceB
MTEQATTTDE
MTEQATTT
MTEQATTTNQ
MTEQATTTNE
MTEQATTTDQ
MTEQAAAADE
AceA
AceA
AceB AceA
FumC
MNTVRSEKDS
MNTVRSQKNS
YjbJ
MNKDE
MNKNQ
MNKNE
MNKDQ
MNADE
HchA
M(7)PQVDIAEDNAFF
M(7)PQVDIAQNNAFF
FrdD
MINPNPKRSDEPVF
MINPNPKRSNQPVF
ElaB
MSNQFGDTRIDDD
MSNQFGDTRINNN
RraB
MNAPEQLEEQ
MNAPEQLQQQ
0
0.5
1
ΔettA / WT normalized YFP intensity
b
MTEQATTTDE
MTEQATTTNQ
p = 0.0004
5'UTR aceB1-10aa yfp
MNKDE
MNKNQ
p = 0.0020
5'UTR yjbJ1-5aa yfp
MANPEQLEEQ
MANPEQLQQQ
p = 0.0010
5'UTR rraB1-10aa yfp
0
0.5
1
Ratio YFP intensity - / + EttA
c
AceB1-10aa
AceB-NQ1-10aa
MTEQATTTDE
MTEQATTTNQ
5'UTR aceB1-10aa yfp1-64aa NV
1 2 3 4 5 6 7 8 Lane
Ribosomes
Retapamulin
Thiostrepton
mRNA1-10aa
mRNA-NQ1-10aa
Buffer
His6-EttA
His6-EttA-EQ2
G A U C
Initiation complex
Arrested elongation complex
d
YjbJ1-5aa
YjbJ-NQ1-5aa
MNKDE
MNKNQ
5'UTR yjbJ1-5aa yfp1-64aa NV
1 2 3 4 5 6 Lane
Ribosomes
mRNA1-5aa
mRNA-NQ1-5aa
Buffer
His6-EttA
His6-EttA-EQ2
G A U C
Initiation complex
Arrested elongation complex

Figure 3

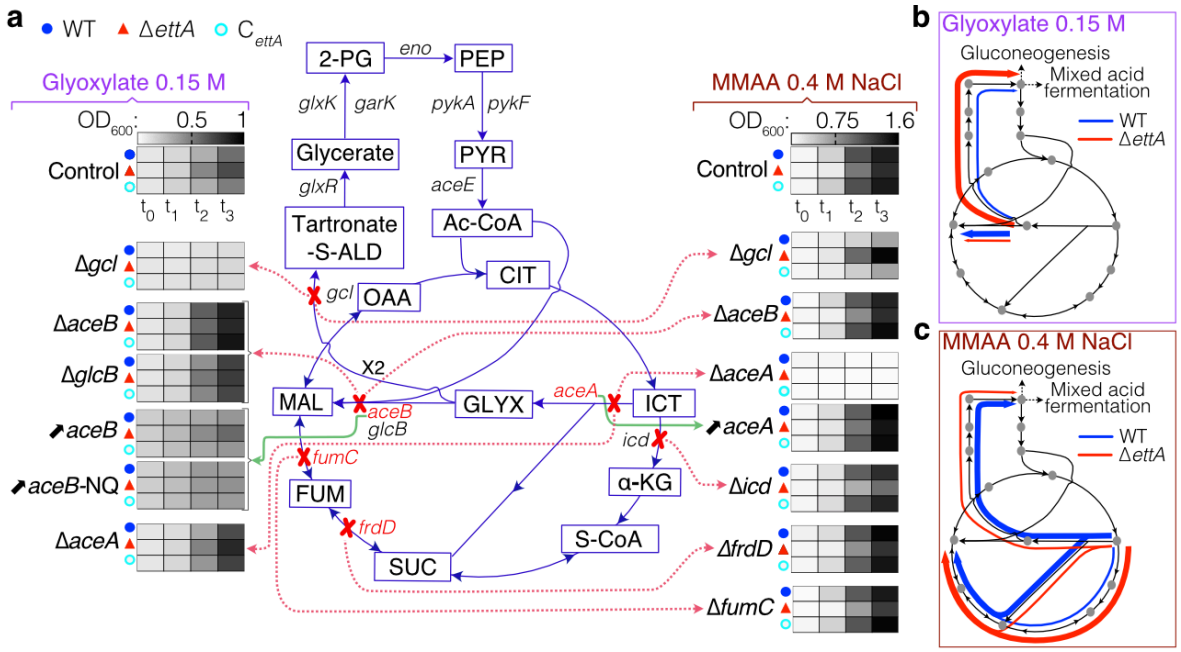
a
WT
ΔettA
C ettA
Glyoxylate 0.15 M
OD600: 0.5 1
Control
t0 t1 t2 t3
Δgcl
ΔaceB
ΔglcB
aceB
aceB-NQ
ΔaceA
2-PG
eno
PEP
glxK
garK
pykA
pykF
Glycerate
PYR
glxR
aceE
Tartronate -S-ALD
Ac-CoA
CIT
gcl
OAA
X2
MAL
aceB
glcB
GLYX
aceA
ICT
fumC
icd
FUM
α-KG
frdD
S-CoA
SUC
MMAA 0.4 M NaCl
OD600: 0.75 1.6
Control
t0 t1 t2 t3
Δgcl
ΔaceB
ΔaceA
aceA
Δicd
ΔfrdD
ΔfumC
b
Glyoxylate 0.15 M
Gluconeogenesis
Mixed acid fermentation
WT
ΔettA
c
MMAA 0.4 M NaCl
Gluconeogenesis
Mixed acid fermentation
WT
ΔettA

Figure 4

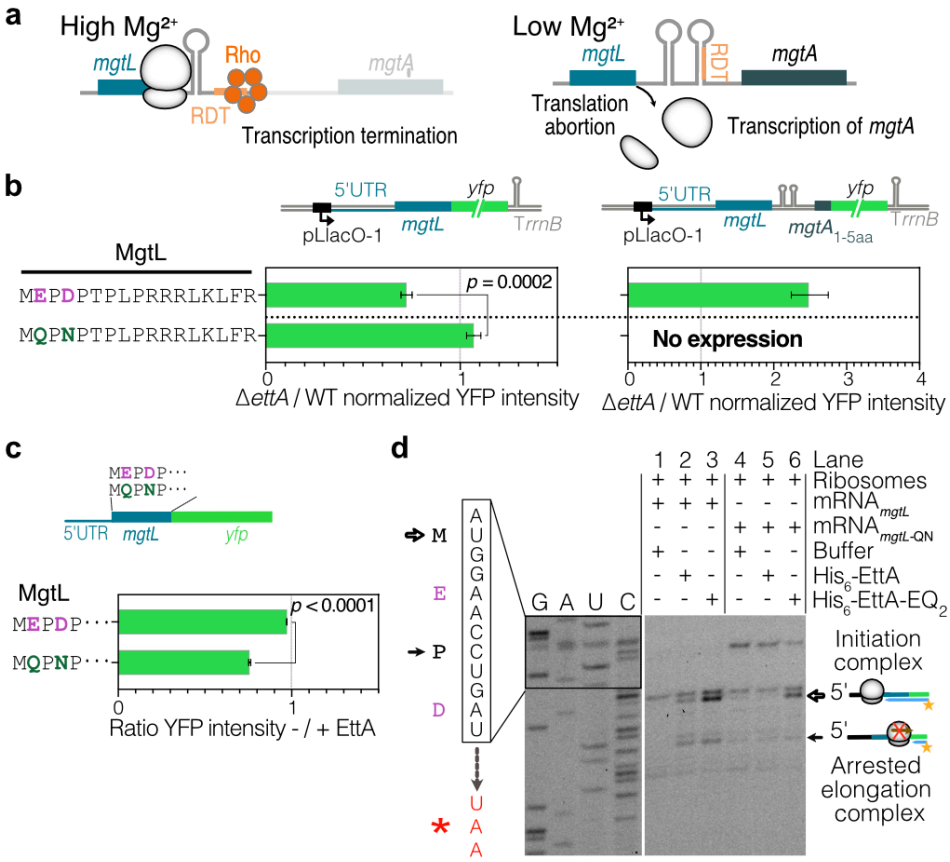
a
High Mg2+
mgtL
Rho
RDT
mgtA
Transcription termination
Low Mg2+
mgtL
RDT
mgtA
Translation abortion
Transcription of mgtA
b
5'UTR
yfp
pLlacO-1
mgtL
TrrnB
5'UTR
yfp
pLlacO-1
mgtL
mgtA1-5aa
TrrnB
MgtL
MEPDPTPLPRRRLKLFR
MQPNPTPLPRRRLKLFR
p = 0.0002
No expression
0
1
ΔettA / WT normalized YFP intensity
0
1
2
3
4
ΔettA / WT normalized YFP intensity
c
MEPDP···
MQPNP···
5'UTR
mgtL
yfp
MgtL
MEPDP···
MQPNP···
p < 0.0001
0
1
Ratio YFP intensity - / + EttA
d
1 2 3 4 5 6 Lane
Ribosomes
mRNAmgtL
mRNAmgtL-QN
Buffer
His6-EttA
His6-EttA-EQ2
M
E
P
D
*
AUGGAACCUGAU
UAA
G A U C
Initiation complex
5'
5'
Arrested elongation complex

Figure 5

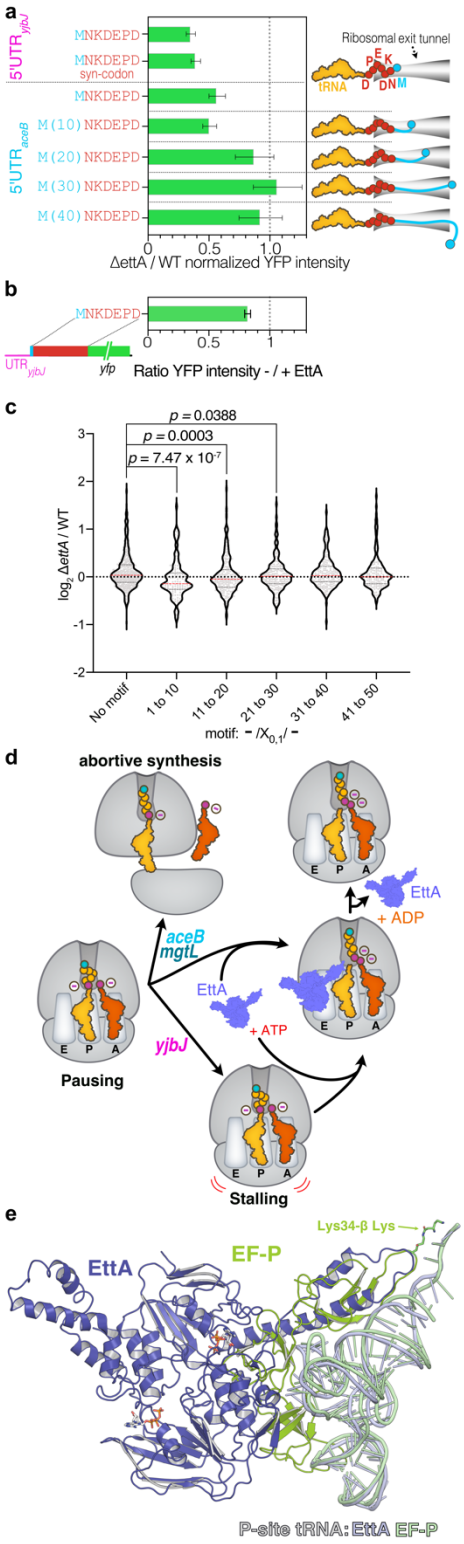
a
5'UTR yjbJ
MNKDEPD
MNKDEPD
syn-codon
MNKDEPD
5'UTR aceB
M(10)NKDEPD
M(20)NKDEPD
M(30)NKDEPD
M(40)NKDEPD
Ribosomal exit tunnel
tRNA
0
0.5
1.0
ΔettA / WT normalized YFP intensity
b
MNKDEPD
UTR yjbJ
yfp
0
0.5
1
Ratio YFP intensity - / + EttA
c
p = 0.0388
p = 0.0003
p = 7.47 x 10-7
log2 ΔettA / WT
No motif
1 to 10
11 to 20
21 to 30
31 to 40
41 to 50
motif: - /X0,1/ -
d
abortive synthesis
aceB
mgtL
yjbJ
EttA
+ ADP
+ ATP
Pausing
Stalling
e
EttA
EF-P
Lys34-β Lys
P-site tRNA: EttA EF-P